Workshops

Modeling of plasma-materials interactions

Inclusion of Nozzle Dimensional Change due to PTFE Ablation in Switching Arc Simulation

J. D. Yan

Department of Electrical Engineering and Electronics, the University of Liverpool, Brownlow Hill, Liverpool, L69 3GJ, the U.K.

Ablation modelling in High Voltage circuit-breakers:

impact on the arc extinction

Ph Robin-Jouan

General Electric Grid Solutions
Villeurbanne, 69100, France

Importance to take into account the wall erosion in CB
Geometric erosion: to be implemanted

Ablation modelling for C2F4

To get vapour:
Heating to vaporization +Latent heat + required energy
to get Teflon in photo dissociation:

(vapour rate) (Hv + Eint3500-Eint1000) = incident radiative Flux

Clausius-Clapeyron Equation and allows us to estimate the vapor temperature at another pressure

$$T_w = -T_c e^{P_w/P_c}$$

Where $P_c = 1.84 \times 10^{15}$Pa, $T_c = 20813$K, and P_w is approximate to the pressure of the neighboring chamber cell [9]. (Mikellides 1999)

Tw will affect hv and Eint1000

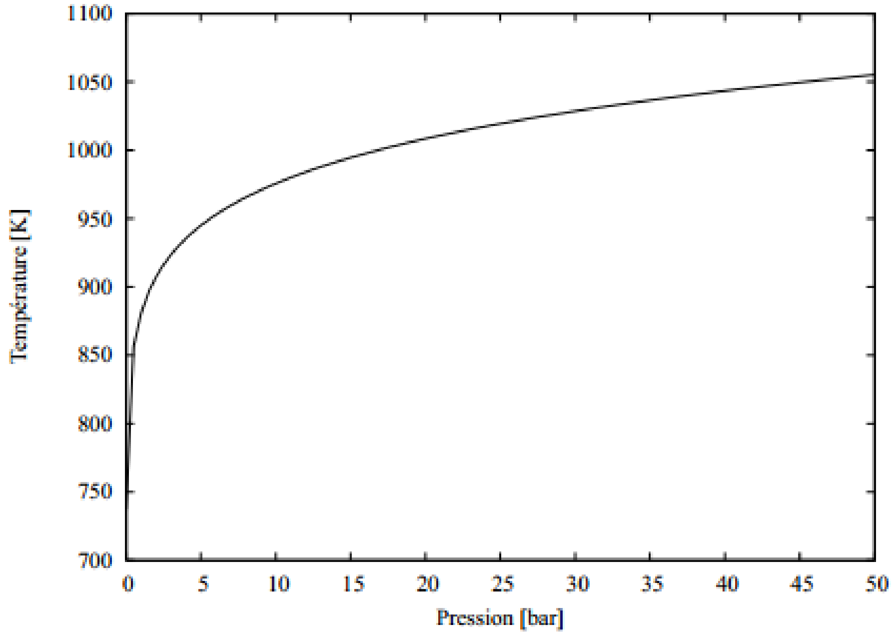

Tw vs pressure for PTFE (Clausius-Clapeyron)

Ablation modelling for C2F4

Experiment: arc confined in a small tube, with length of 75 mm and radius of 6 mm.

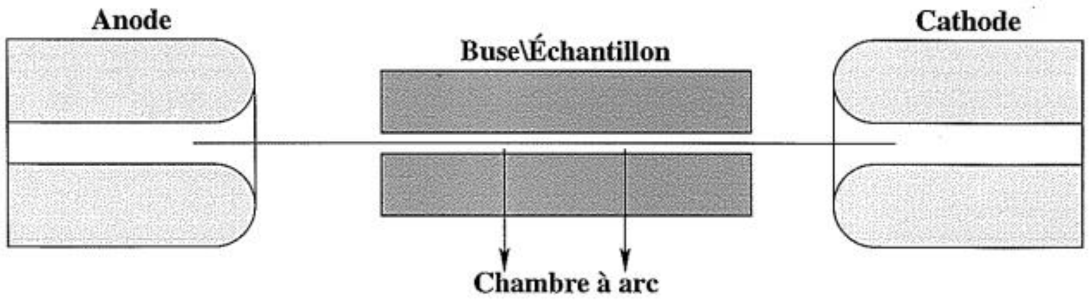

CFD 2004: SOLUTION OF MUL TI-SPECIES REAL GAS FLO WS
WITH ELECTRIC ARC AND W ALL ABLA TION
Alexandre Martin, Marcelo Reggio, Jean-Yves Trépanier, EPM

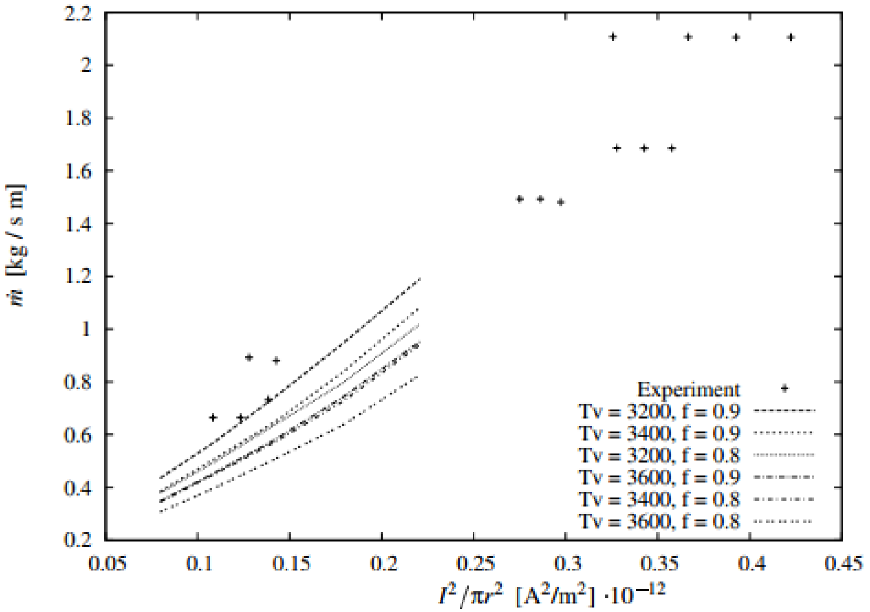

Figure 7: Ablation rate as function of arc current I and tube radius r, for different value of f and T_v; comparison with experimental values obtained by Ruchti

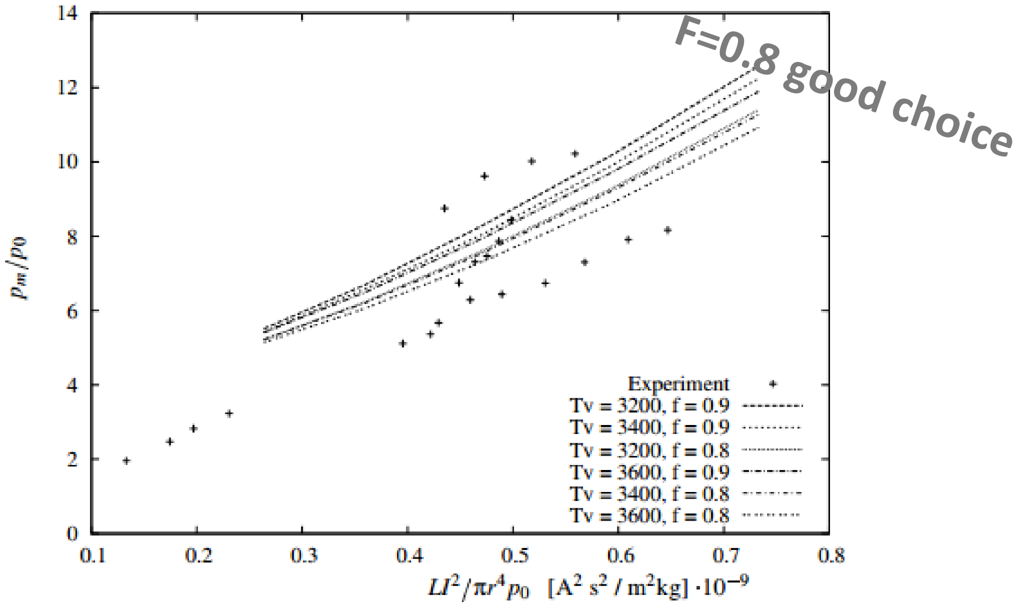

Figure 8: Total Pressure as a function of tube length L, tube radius r, exhaust pressure p_0 and arc current I, for different value of f and T_v; comparison with experimental values obtained by Ruchti

Ablation modelling for C2F4: geometric erosion

The applied current cycle is repeated in **10 consecutive** times to predict the changes in the nozzle mass flux in a long-operation time. In the present simulation, the peak current is **56kA** and the arcing time for each cycle **is 6.4ms**.

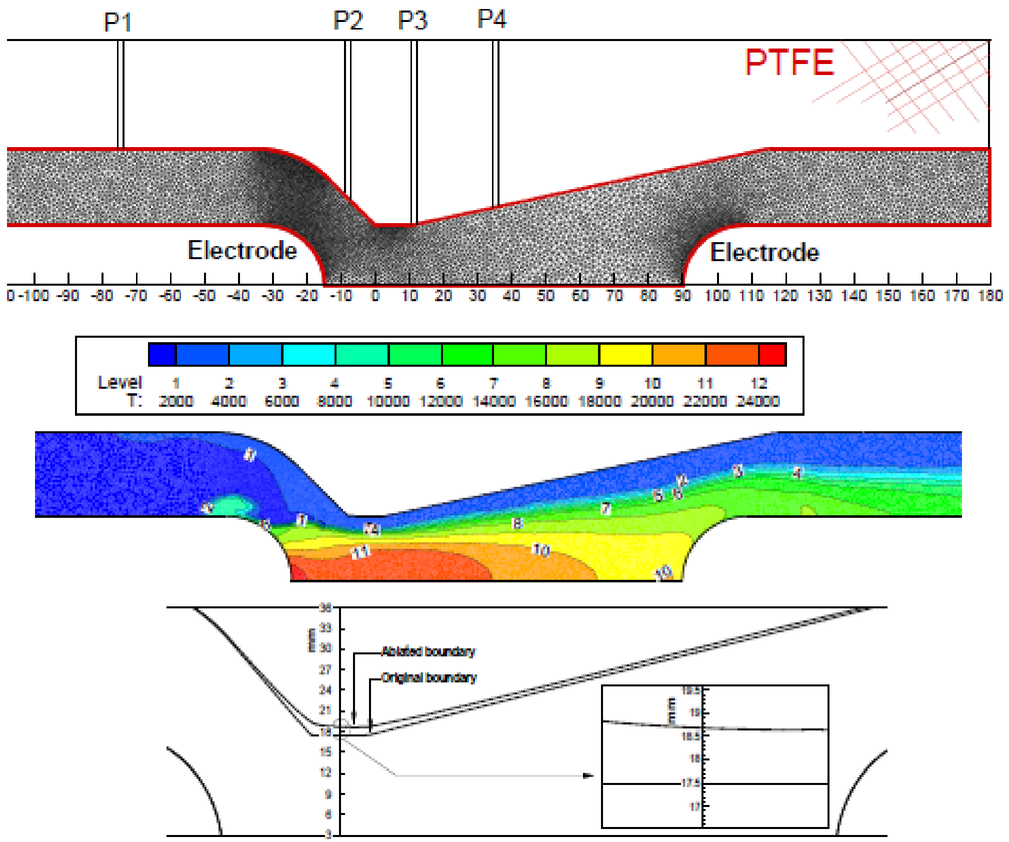

Fig. 12: *Geometry change after applying 10 current cycle.*

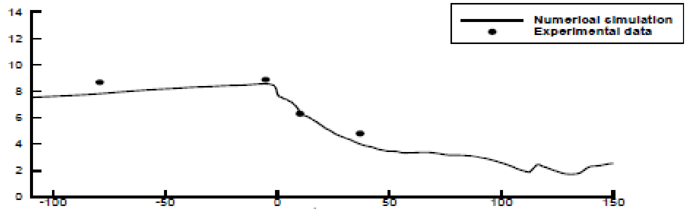

Fig. 6: *Axial pressure distribution at, t=7ms, I=26.4 kA.*

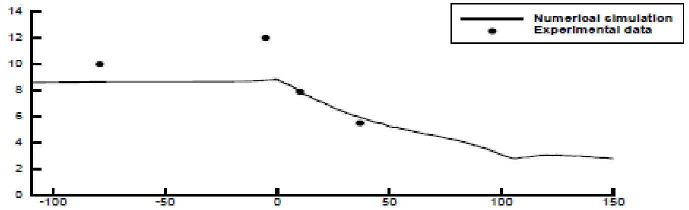

Fig. 7: *Axial pressure distribution at, t=9ms, I=55.7 kA.*

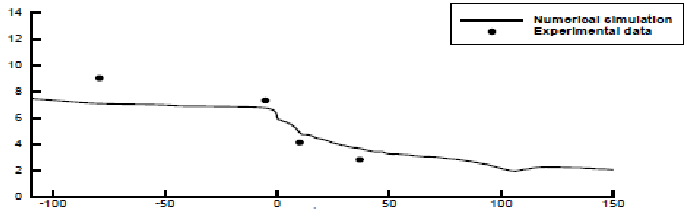

Fig. 8: *Axial pressure distribution at, t=11ms, I=35.5 kA.*

Prévision des paramètres de géométrie pour la soudure

Couplages dans le modèle

- Wire/droplet
- Welding arc
- Anode and cathode layer
- Weld pool including free surface and heat and mass transfer
- Solidification

Heat input at cathode layer : commonly modeled as axisymmetric or elliptic Gaussian distribution

Hypothesis:

* Cathode area consists of elementary cathode spots (CS)
* Processes of CS are highly depended on evaporation
*** Interface "droplet-arc"** requires heat and current fluxes distribution on surface of droplets due to the arc actions.
*** Interface "arc-weld pool"** requires heat, current, mass fluxes and pressure distribution on the weld pool surface due to the arc and droplets actions.

$I{\sim}200A; U{\sim}20V; v_w{\sim}50 - 100 cm/min$; S355 Ar

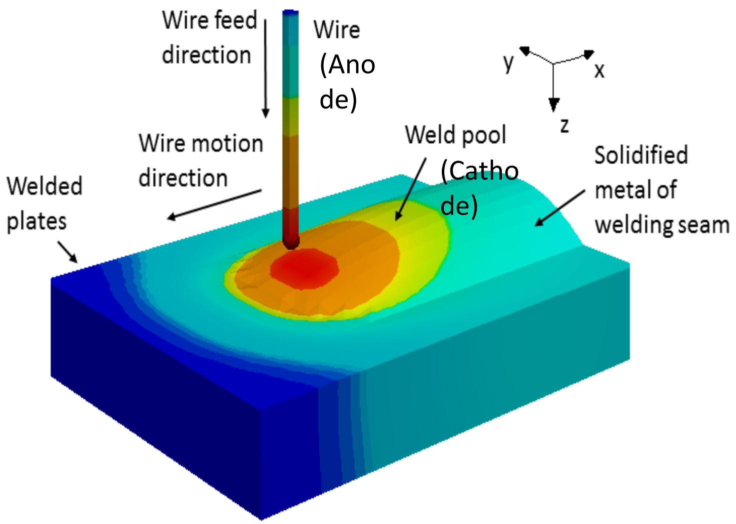

- Model for elementary CS, taking into account evaporation was developed
- Model for distribution of CS was developed, using a simplified temperature modification model

Result:

Temperature profile, heat flux evolution in cathode area

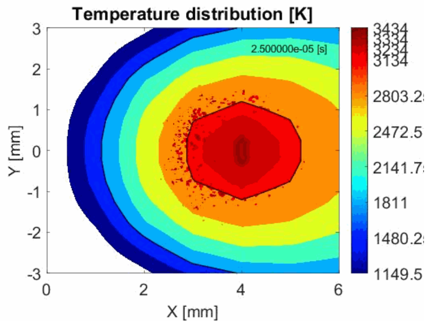

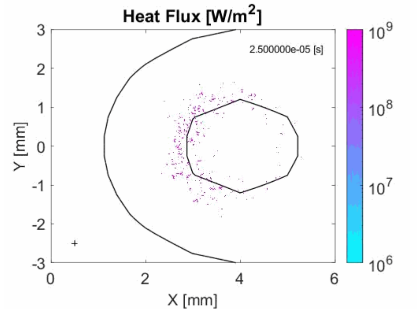

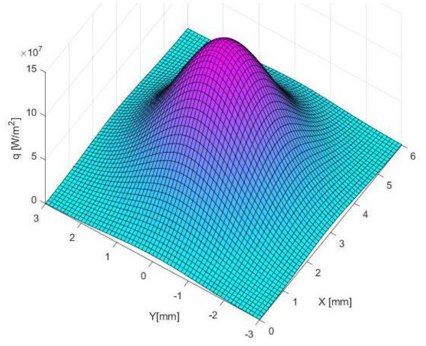

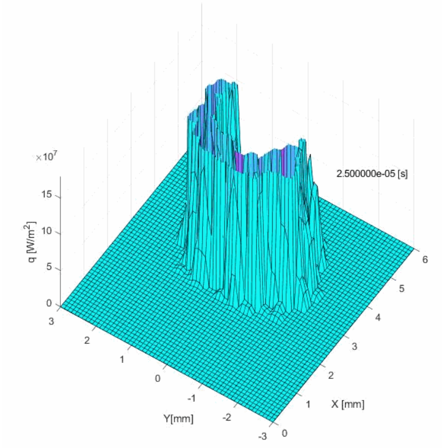

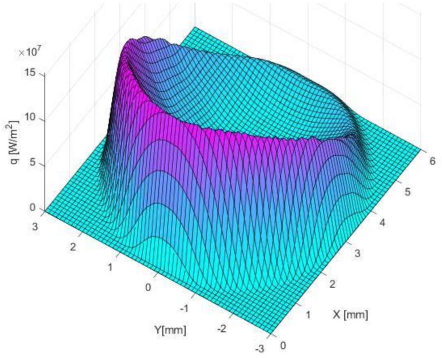

Conclusion:

When evaporation is taken into account, the heat flux distribution might be modified and non-axisymmetric

Outlook:

Coupling to hydrodynamic weld pool simulation

Impuls-process and dip-transfer

PROPERTIES STUDIES

1/ COMPARISON OF CALCULATED TRANSPORT PROPERTIES WITH MEASUREMENTS IN A WIDE PRESSURE RANGE

2/LAST DEVELOPMENT RESULTS FOR 170kV CIRCUIT-BREAKER PROJECT USING g3 GAS

3/NUMERICAL STUDY ON CO2 GAS CIRCUIT BREAKER USING SEMI-EMPIRICAL MODEL FOR RADIATIVE ENERGY TRANSFER

4/RADIATIVE TRANSFER CALCULATION OF CO2 THERMAL PLASMA USING A HYBRID PLANCK-ROSSELAND MEAN ABSORPTION COEFFICIENT

5/DIELECTRIC PROPERTIES OF HOT C5F10O AND ITS MIXTURES WITH CO2 AT THE ELEVATED TEMPERATURE

6/CHEMICALLY NON-EQUILIBRIUM STATE IN SF6 ARC PLASMAS DUE TO THE VARIATION AND SPATIAL GRADIENT IN TEMPERATURE

7/PRESSURE DEPENDENCE OF THE OPTIMIZED MEAN ABSORPTION COEFFICIENTS

8/SYSTEMATIC INVESTIGATION ON RADIATION MODELING ERRORS OF A WALL-STABILIZED ARC SIMULATIONS

9/COMPARISON OF DIFFERENT MODELS TO CALCULATE THE COMPOSITION AND THERMODYNAMIC PROPERTIES OF A MULTI-TEMPERATURE SF6 PLASMA

COMPARISON OF CALCULATED TRANSPORT PROPERTIES WITH MEASUREMENTS IN A WIDE PRESSURE RANGE

T. RUNGE, ST. FRANKE, S. GORTSCHAKOW, R. METHLING AND M. KURRAT

Etude : comparaison calculs-mesures de σ(T,P) dans un plasma d'air pour hautes T°(30000K) et hauts P° (500 bar)
Conclusion : σ(T,P) mesurée est différente de σ(T,P) calculée

Procédure
1/Mesure de la température, de la pression et de la conductivité électrique du plasma (Fig1.3)
2/Détermination de la température à partir du calcul des propriétés de transport, connaissant la pression et la conductivité électrique mesurées
3/Comparaison des températures mesurées (1) et calculées (2)

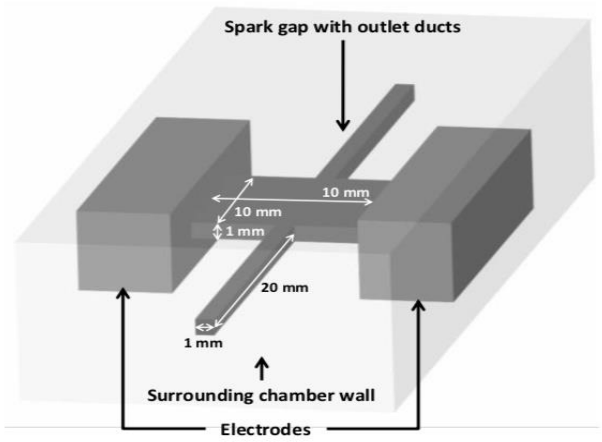

Fig. 1. 3-D model of the spark gap model without SDD [8].

Impulse currents 8/20 µs, Amplitudes up to 23 kA
Électrodes CuW
Chambre Wall en POM

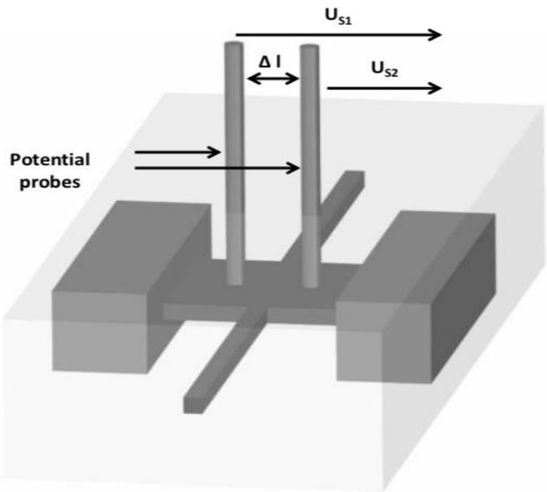

Fig. 2. Measuring set-up for electrical conductivity [8].

$$\sigma = \frac{j * \Delta l}{U_{P1} - U_{P2}}$$

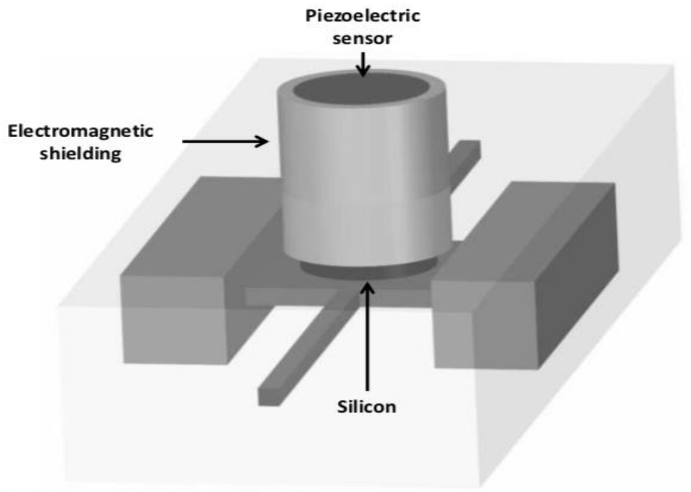

Fig. 3. Measuring set-up for plasma pressure.

Méthode piezoélectrique

COMPARISON OF CALCULATED TRANSPORT PROPERTIES WITH MEASUREMENTS IN A WIDE PRESSURE RANGE

T. RUNGE, ST. FRANKE, S. GORTSCHAKOW, R. METHLING AND M. KURRAT

Mesure de la température : OES (Lorentz fit de la raie H_α à faibles courants, comparaison corps noir à forts courants)
Calcul de la la température : report de la conductivité électrique calculée sur la courbe théorie σ(T,P) d'un plasma d'air

Mesure de conductivité électrique : $\sigma_{max} = 170 * j_{max}{}^{0,74}$ à $\pm$20%

Mesure de la pression (par capteur piézoélectrique): $p_{max} = 4.63 * \frac{j_{max}{}^2}{\sigma_{max}}$ à $\pm$ 30%

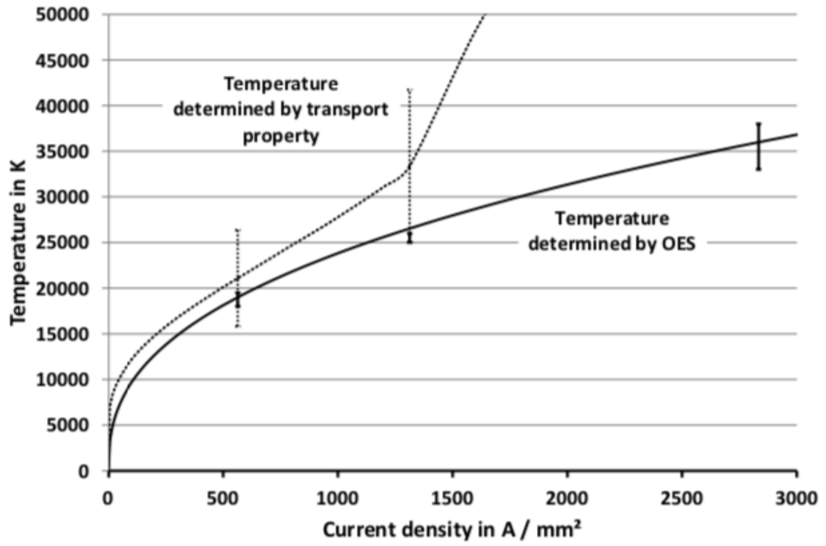

Fig. 6. Comparison of the determined temperatures in dependence of current density.

Méthode de calcul est cohérente si J<1300 A/m²

Raisons:
- Non LTE
- Non ideality effects (basses T°, hautes P°)
- Non stationnaire plasmas (t<1μs)

LAST DEVELOPMENT RESULTS FOR 170kV CIRCUIT-BREAKER PROJECT USING g3 GAS

H.E. JUNG, K.K. OH, Y.G. KIM, K. BOUSOLTANE, M. PERRET, P. ROBIN-JOUAN, J-Y. TREPANIER, S. ARABI

Etude : développement d’un outil permettant de dimensionner un 170kV GIS
Amélioration design de la chambre afin d’avoir une pression supérieure - remplacement SF_6 par g^3
Comparaison simulation 2D avec expérience pour g^3 dans 170kV CB, 50kA, 60Hz, P<0.5MPa

Modèle : 2D axi, LTE, équations Euler, équations Maxwell, méthode volumes finis
Mesh triangulaire, auto adaptative, non structurée, gaz CO_2

Comparaisons tests-modèle sur V_{arc}(t), P°(t), I(t) et masse ablatée pour t_{arc} court (15ms) et long (22ms)

Bon accord entre code et modèle

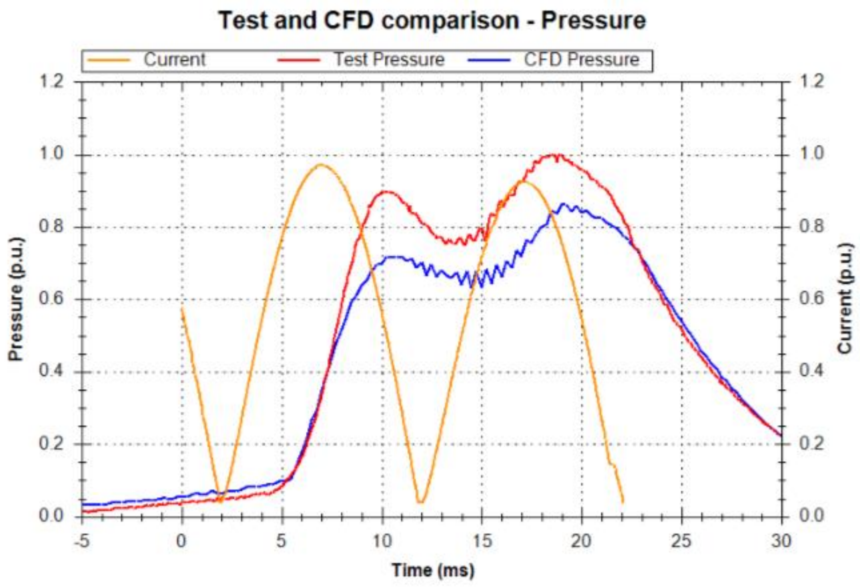

Figure 4 - Test and CFD comparison of pressures in the thermal volume for long arcing time

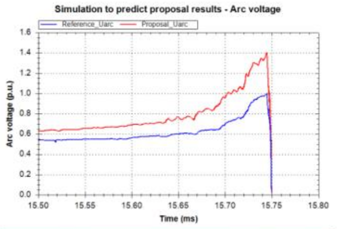

Figure 6 - Comparison of arc voltages from two simulations for short arcing time

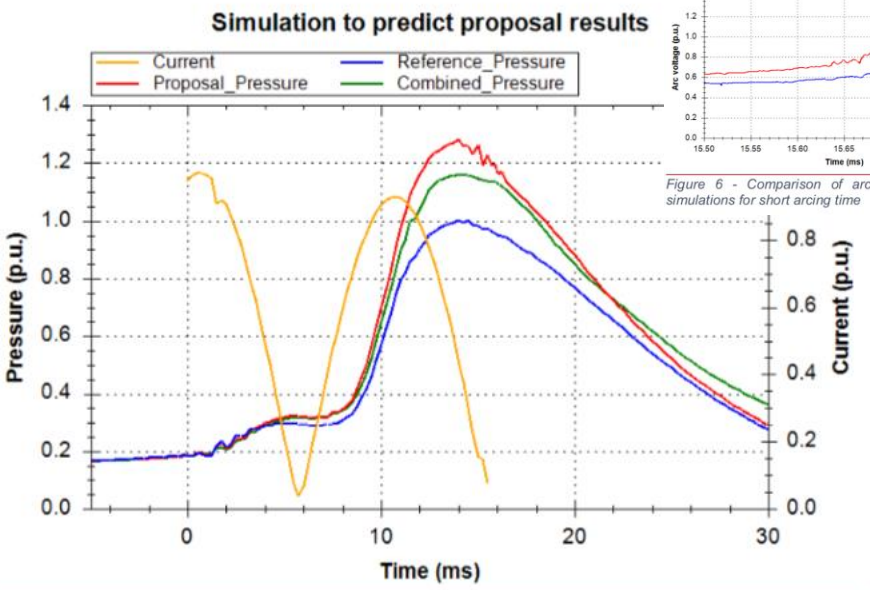

Figure 7 - Comparison of pressures from three simulations for short arcing time

NUMERICAL STUDY ON CO2 GAS CIRCUIT BREAKER USING SEMI-EMPIRICAL MODEL FOR RADIATIVE ENERGY TRANSFER

T. YOSHINO, A. MAJIMA, T. UCHII, T. MORI AND T. FUJINO

Etude : rayonnement dans les CB avec CO_2, étude semi empirique du transfer radiatif
Etude de l'influence sur V_{arc} de la réabsorption du rayonnement sur les bords, autoabsorption, turbulence

Modèle:

Modèle 2D, CO_2, 4.5KA, bon accord sur V_{arc}
Propriétés LTE, ablation PTFE et érosion Cu incluse
Prandtl mix, $Prt = 1.0$, $lm=0.04\delta(z)$

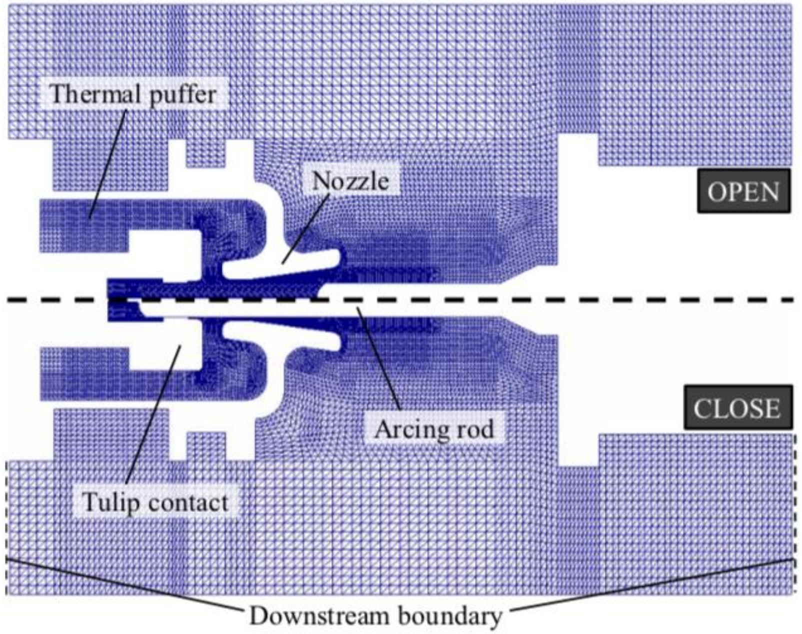

Fig. 4 Geometry of model GCB and computational grid

Rayonnement:

Modèle semi-empirique
réabsorption sur les bords, autoabsorption dans le cœur
Cœur arc : $T_{max}>T>0.8T_{max}$; $\nabla\cdot \boldsymbol{q}_{rad} = (1-C_{self})4\pi\varepsilon$
Bords arc : $4000<T<0.8T_{max}$, $\nabla\cdot \boldsymbol{q}_{rad} = -E_{abs}$
Régions froides : T<4000K, $\nabla\cdot \boldsymbol{qrad} = (1 - Cself)4\pi\varepsilon$

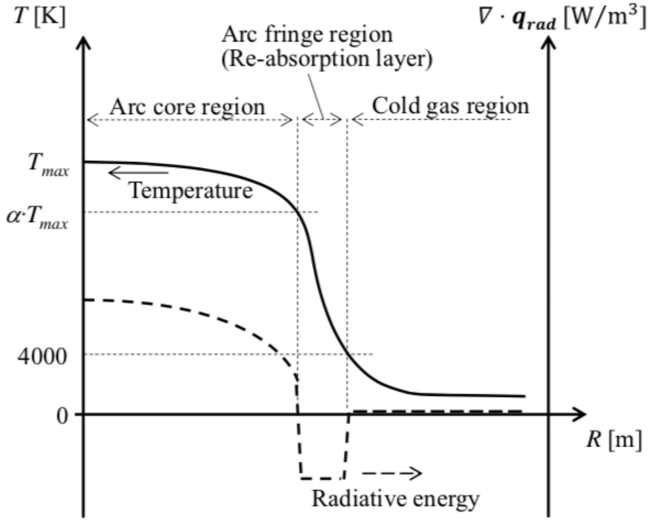

Fig. 2 Schematic view for semi-empirical radiative transfer model

$$E_{abs} = \frac{\int_{V_{emi}} \alpha\cdot(1-C_{self})\cdot 4\pi\varepsilon\, dV}{\int_{V_{abs}} dV}$$

V_{emi} is emission volume of arc core, and V_{abs} is absorption volume of arc fringe

NUMERICAL STUDY ON CO2 GAS CIRCUIT BREAKER USING SEMI-EMPIRICAL MODEL FOR RADIATIVE ENERGY TRANSFER

T. YOSHINO, A. MAJIMA, T. UCHII, T. MORI AND T. FUJINO

Conclusions sur plusieurs tests avec ou sans phénomènes

1/ la turbulence influence V_{arc} si I<2kA proche du zéro de courant
2/ V_{arc} en autoabsorption > V_{arc} sans autoabsorption pour t>12ms
3/ V_{arc} chute si pas de re-absorption sur les bords

Table 1 Using modelling for each simulation case

Simulation case	A	B	C	D
Re-absorption (Absorption in arc fringe)	✓	✓	✓	–
Self-absorption	✓	✓	–	–
Turbulence	✓	–	–	–

Coché signifie que le phénomène est pris en compte dans le test.

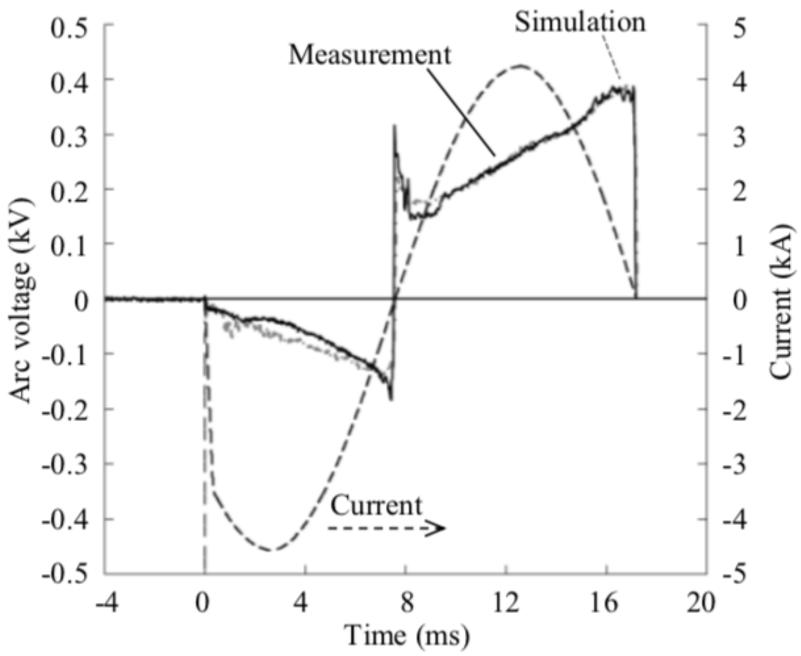

Fig. 6 Comparison of arc voltage between measurement and simulation

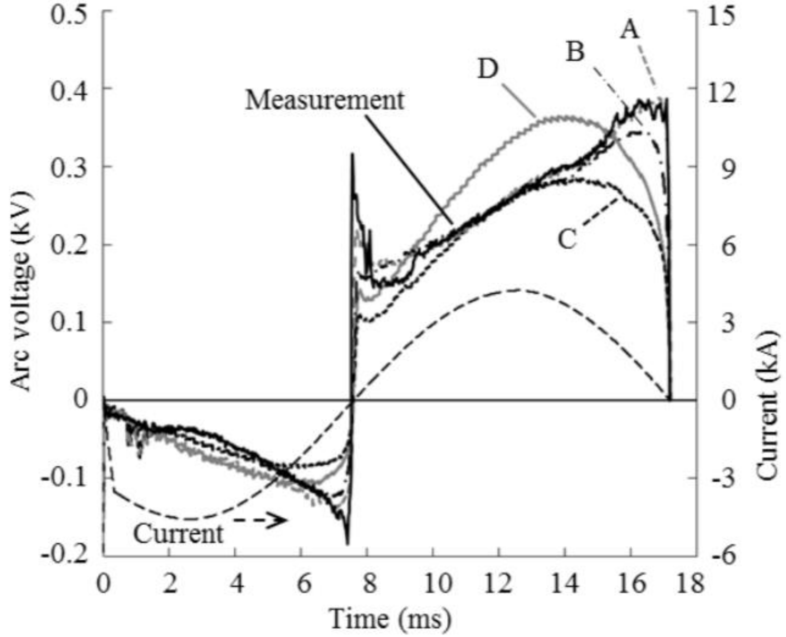

Fig. 7 Influence of arc modelling on arc voltage

RADIATIVE TRANSFER CALCULATION OF CO2 THERMAL PLASMA USING A HYBRID PLANCK-ROSSELAND MEAN ABSORPTION COEFFICIENT

S. KOZU, T. FUJINO, T. YOSHINO, T. MORI

Etude : transfert radiatif dans CO_2 avec hybrid-planck-rosseland MAC (PR)

Constat : la moyenne de Planck (K_P) surestime transfert radiatif, il est fait pour des plasmas optiquement minces

La moyenne de Rosseland (K_R) sous-estime le transfert radiatif, il est fait pour les plasmas optiquement épais

Modèle

Model 1D, T(r) multi bandes, méthode P1+PR (Planck-Rosseland)

Comparaison PR, P, R couplé avec P1+ spectre complet sur 79.714 fréquences (sous-estimé dans $2.2\text{-}2.27.10^{15}$hz)

7 bandes spectrales

Test sur profil T_{max}=20000K, T_{min}=300K, r=0.01m, 0.1MPa

Table1. Relationship between each group and frequency band

Group	ν_i	ν_{i+1}
1	1.00×10^{14}	5.00×10^{14}
2	5.00×10^{14}	1.50×10^{15}
3	1.50×10^{15}	2.20×10^{15}
4	2.20×10^{15}	2.72×10^{15}
5	2.72×10^{15}	3.29×10^{15}
6	3.29×10^{15}	8.49×10^{15}
7	8.49×10^{15}	1.00×10^{16}

Amélioration des MACs par méthode hybride

$$\kappa_H = (1-\gamma)\kappa_P + \gamma\kappa_R$$

$$\gamma = \frac{\kappa_P - \kappa_R}{\kappa_P},$$

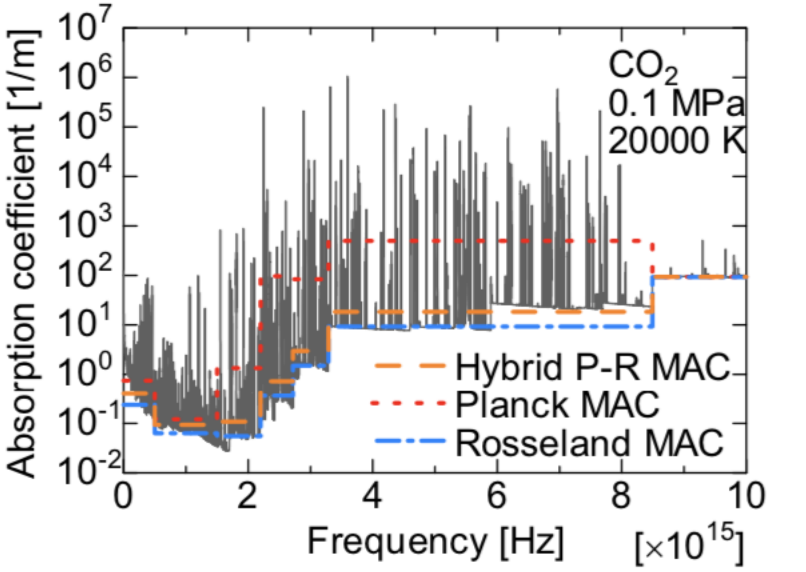

Fig1. Absorption coefficient of CO_2 at temperature of 20000 K and pressure of 0.1 MPa

RADIATIVE TRANSFER CALCULATION OF CO2 THERMAL PLASMA USING A HYBRID PLANCK-ROSSELAND MEAN ABSORPTION COEFFICIENT

S. KOZU, T. FUJINO, T. YOSHINO, T. MORI

Profil de température choisi pour le test

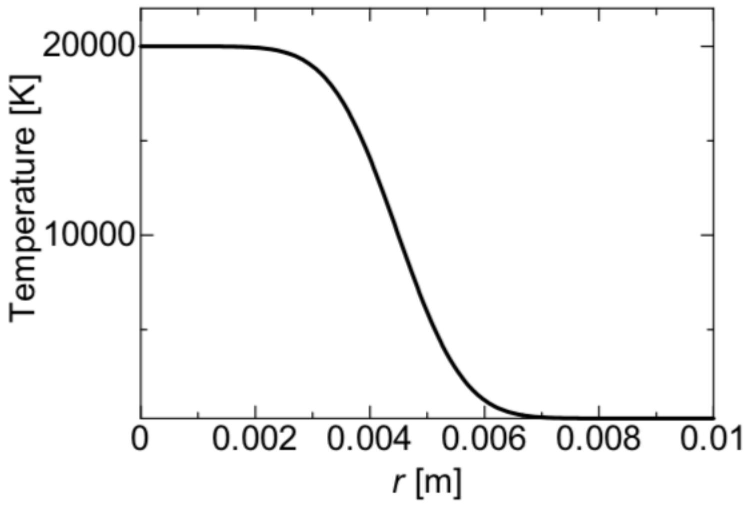

Fig2. Radial temperature profile

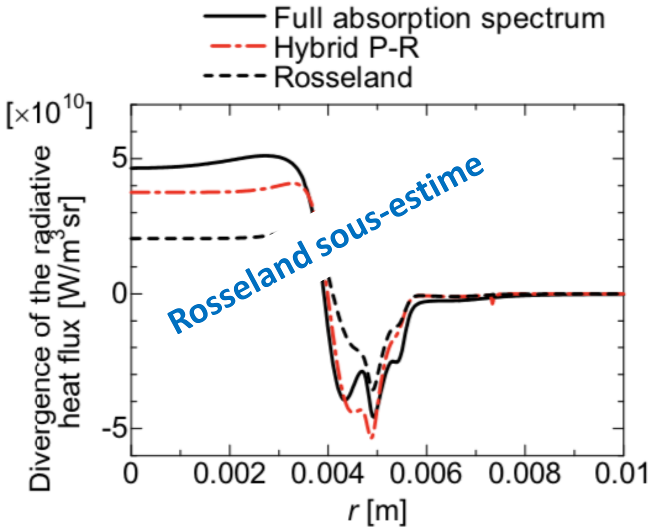

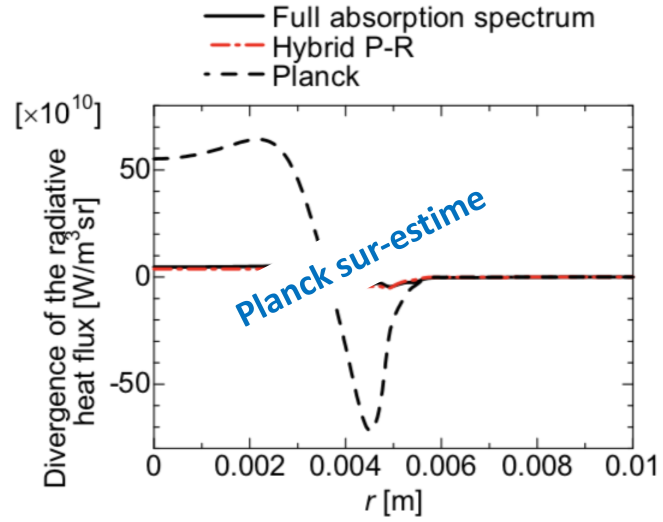

(b)

$2.20 - 2.72 \, 10^{15}$ Hz

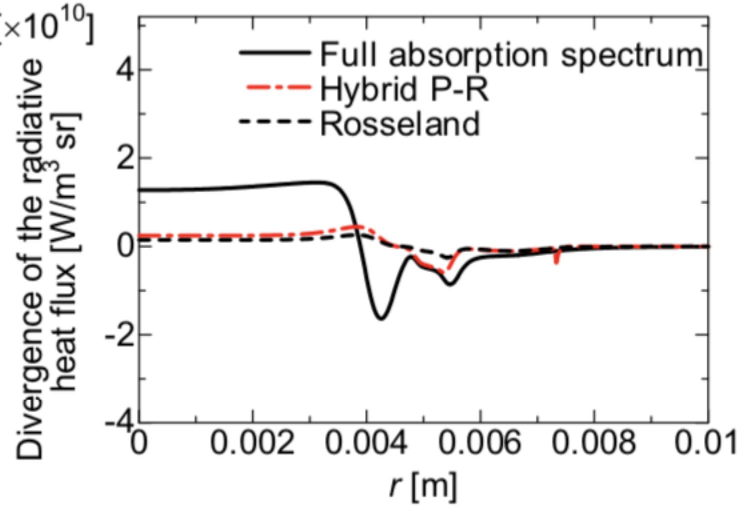

Fig4. Radial distribution of divergence of radiative heat flux (group4)

La valeur de γ dans l'expression de K_H doit être optimisée

DIELECTRIC PROPERTIES OF HOT C5F10O AND ITS MIXTURES WITH CO2 AT THE ELEVATED TEMPERATURE

X.X. GUO, J.Y. XIONG, X.W. LI, B.X. LI AND L. CHEN

Etudes : propriétés diélectriques des mélanges $C_5F_{10}O$ + CO_2 à haute températures et hautes pressions (P=1-8atm, T=300-4000K)

Compo ETL -> Comsol+LXCAt -> EEDF -> α, η -> $(E/N)_{Critique}$

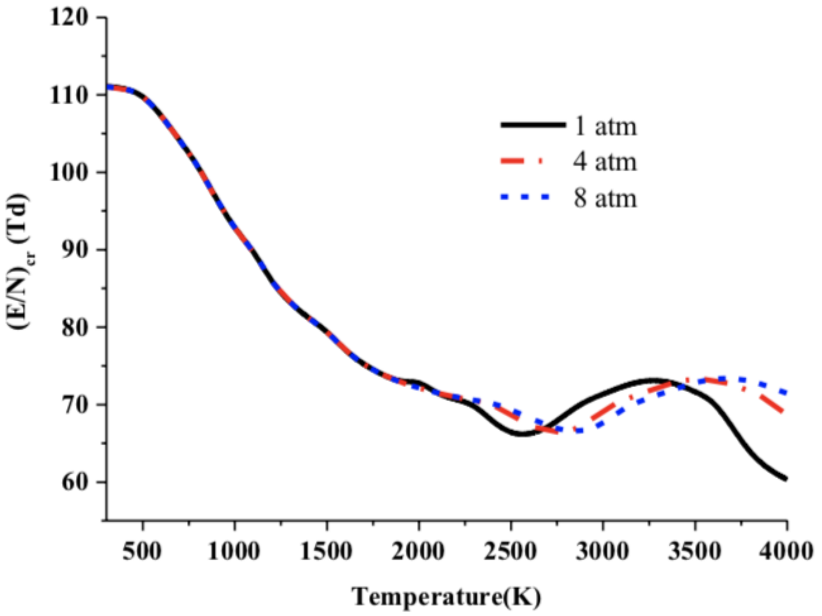

Fig.5 Critical reduced electric field strength $(E/N)_{cr}$ in hot 10%$C_5F_{10}O$-90%CO_2 at different gas pressures as a function of gas temperature

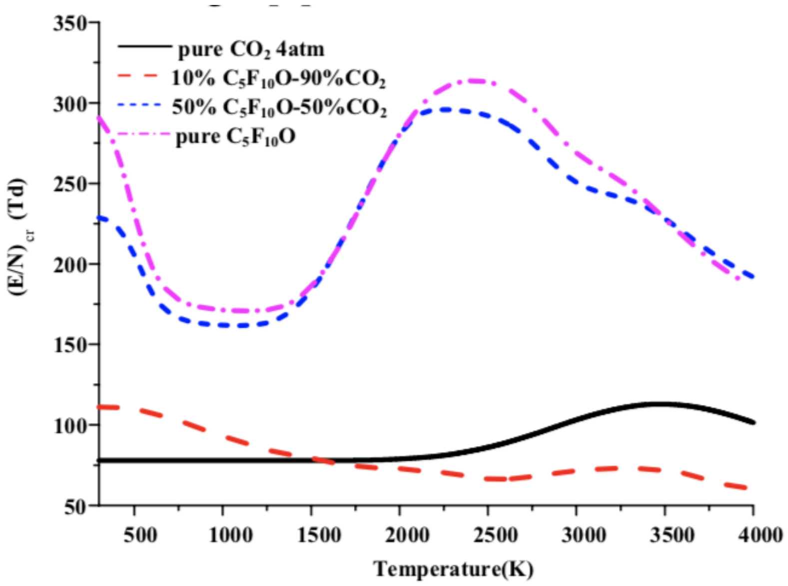

Fig.6 Critical reduced electric field strength $(E/N)_{cr}$ in hot pure $C_5F_{10}O$ and 10%$C_5F_{10}O$-90%CO_2 at 1atm (pure CO_2 at 4atm) and at different gas pressures as a function of gas temperature

Conclusions :

Avec de faibles vapeurs de $C_5F_{10}O$: E/N augmente pour T<1000K, E/N diminue pour T supérieure

Avec de fortes vapeurs de $C_5F_{10}O$ (+50%) : E/N est plus grand

CHEMICALLY NON-EQUILIBRIUM STATE IN SF6 ARC PLASMAS DUE TO THE VARIATION AND SPATIAL GRADIENT IN TEMPERATURE

Y. TANAKA & T. IIJIMA

Etudes : identification des région en Non-LCE dans le temps et dans l'espace

Modèle d'un arc en extinction : arc SF_6, 19 espèces, 122 réactions, avec équation de conservation des espèces

Étude de l'influence du gradient de T dans le temps (dT/dt) et dans l'espace (dT/dr) sur Ne

Résultats avec variation de (dT/dt) de 10 à 1000μK/μs

La prise en compte des déséquilibres chimiques temporellement affecte Ne pour T<6000K

SF_6 uniforme spatialement par comparaison avec une composition à LTE

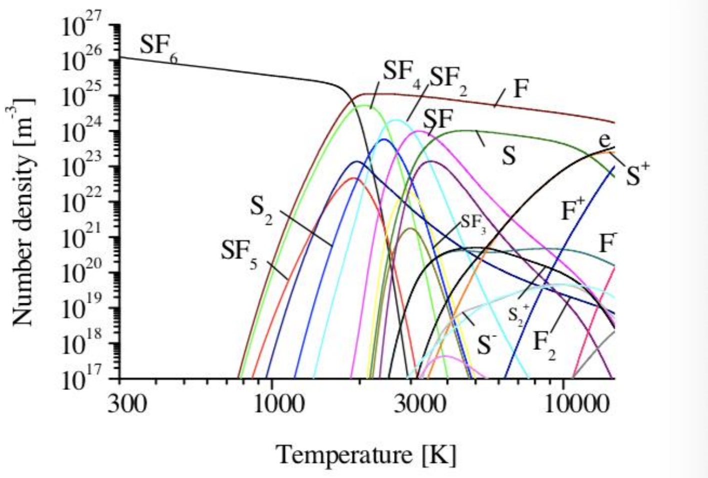

Fig. 1. Particle composition of SF_6 at a pressure of 0.5 MPa under equilibrium condition.

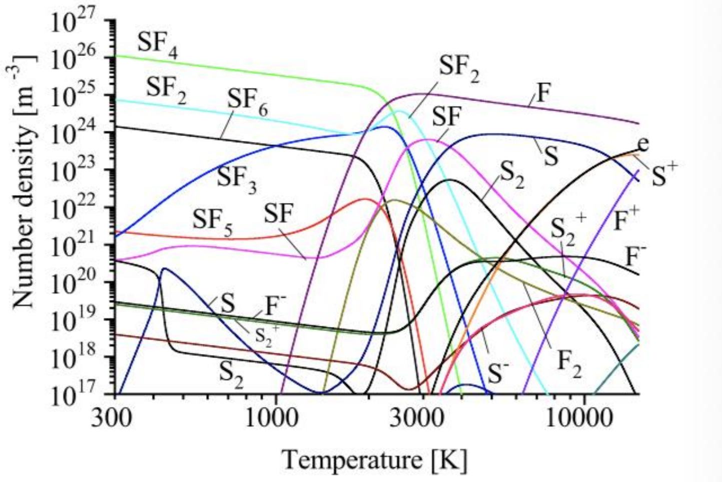

Fig. 2. Composition change as a function of temperature with of decay rate of $dT/dt = -10$ K/μs.

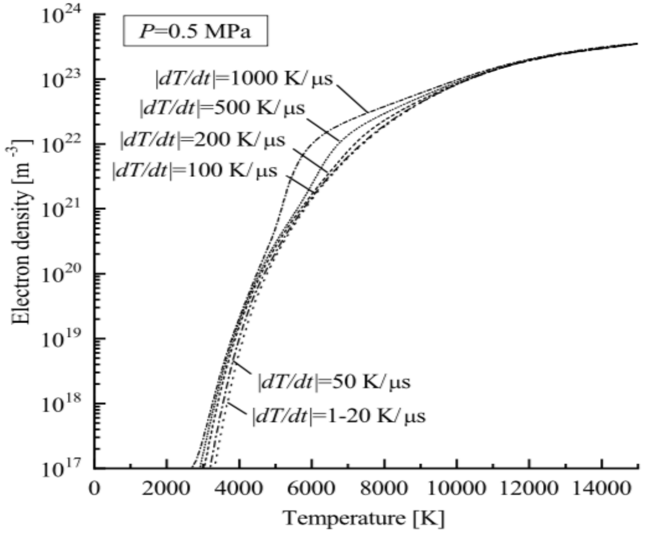

Fig. 3. Electron density variation as a function of temperature at different decay rates dT/dt at 0.5 MPa.

CHEMICALLY NON-EQUILIBRIUM STATE IN SF6 ARC PLASMAS DUE TO THE VARIATION AND SPATIAL GRADIENT IN TEMPERATURE

Y. TANAKA & T. IIJIMA

Résultats avec variation de (dT/dr) de 10^6 à 10^8K/m

La prise en compte des déséquilibres chimiques spatialement affecte Ne pour T<4000K

Distribution spatiale permet d’identifier les régions de non-LCE

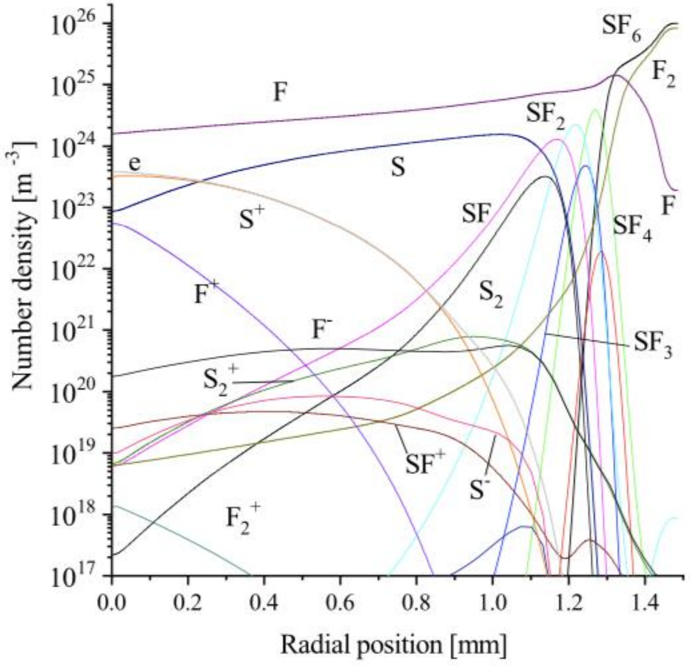

Fig. 5. Radial distribution of SF_6 composition with a radial gradient of $|dT/dr| = 10^7$ K/m at 0.5 MPa.

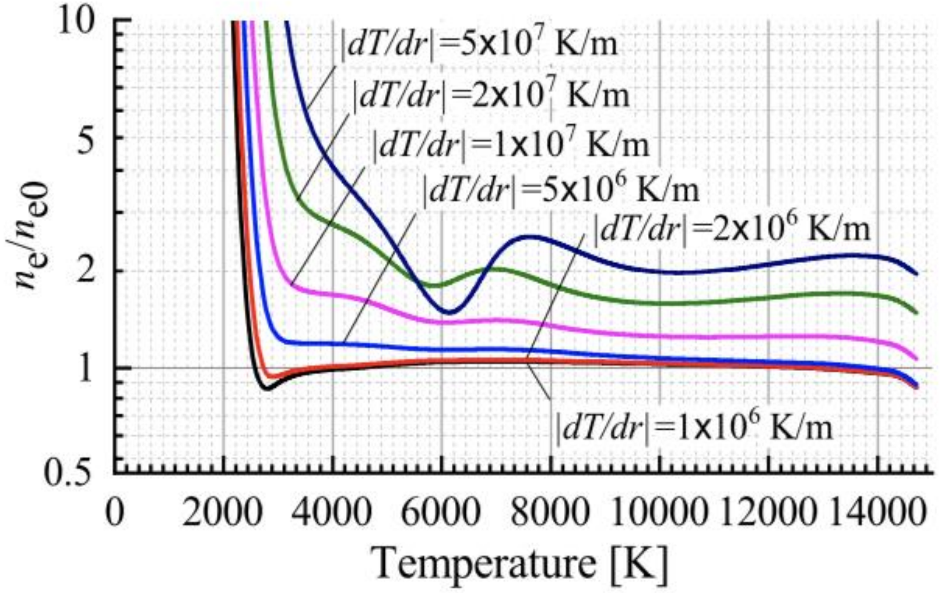

Fig. 6. Electron density ratio n_e/n_{e0} in SF_6 plasma at 0.5 MPa for different gradient $|dT/dr|$'s.

PRESSURE DEPENDENCE OF THE OPTIMIZED MEAN ABSORPTION COEFFICIENTS

P. KLOC, V. AUBRECHT, M. BARTLOVA

Etudes : Optimisation des MACs pour une bonne modélisation du transfert radiatif dans l'air
Détermination de la divergence du flux rayonné (résolution exacte, et approchée)
Utilisation de la moyenne de Planck modifiée (utilisation du paramètre H longueur caractéristique et non plus R_p)
(Papier précédent $H=2R_p$ mais ici plutôt $H=3R_p$ mais quand pression augmente, on ne sait pas)

Objectifs :
Détermination des bandes spectrales en fonction de la pression (et non plus supposée constantes en fonction de la pression)

Paramètres :
Plasmas d'air, pression de 0.5 bar jusqu'à 5 bar
Test de 2 profils, 6 pressions, 3 bandes
Utilisation d'une fonction optimisation

→

$$\Delta F = \frac{\sum_{i=1}^{20} (\nabla \cdot F\text{ex}_{,i} - \nabla \cdot F\text{mac}_{,i})^2}{\sum_{i=1}^{20} \nabla \cdot F^2_{\text{ex},i}}$$

Conclusions :
$H = 3R_p$
$L_1=2.93759 \times 10^{15}$hz
$L_2=3.51299 \times 10^{15}$Hz
Valable jusqu'à 5bar

p (bar)	$n = 7$		$n = 100$	
	H_b (cm)	$x \cdot R_p$	H_b (cm)	$x \cdot R_p$
0.5	1.6	3.46	0.65	3.41
1.0	1.5	3.24	0.65	3.41
2.0	1.5	3.24	0.55	2.88
3.0	1.6	3.46	0.55	2.88
4.0	1.8	3.89	0.55	2.88
5.0	2.1	4.54	0.60	3.15

p (bar)	$n = 7$		$n = 100$	
	ΔF_b	ΔF_g	ΔF_b	ΔF_g
0.5	17.7	17.7	19.3	19.8
1.0	11.0	11.0	14.2	14.3
2.0	7.8	7.8	9.9	9.9
3.0	6.5	6.9	8.2	8.2
4.0	4.6	6.4	7.0	7.1
5.0	3.1	6.4	6.2	6.6

SYSTEMATIC INVESTIGATION ON RADIATION MODELING ERRORS OF A WALL-STABILIZED ARC SIMULATIONS

R. FUCHS, H. NORDBORG

Etudes : transfert radiatif – comparaisons des méthodes dégénérées pour le SF_6

Objectifs : déterminer le nombre de bandes pour bien décrire la tension d'arc et T(r) dans un modèle

Nouveautés :

Utilisation des moyennes de Rosseland, Planck, Renormalisée

Traitement particulier du coefficient d'absorption des raies

$$\kappa_{\nu,line} = \frac{1}{h}(1 - \exp(-\kappa_{\nu,line}h)),$$

7 bandes : 0.066, 0.35, 1.54, 2.65, 2.94, 3.52 × 10^{15}Hz

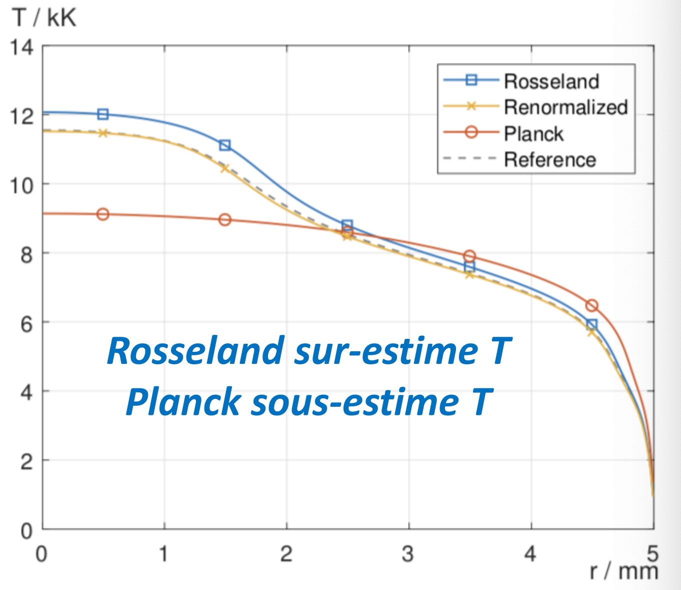

Fig. 1: Temperature profiles for low number of spectral bands.

Modèle numérique

LTE arc stabilisé SF_6 cylndrique

I=100A, 400 pts

T_{wall}=300K, r_{wall}=5mm, P=10bar

7 bandes (Modèle P1)

P et E uniforme

Faible convection

Température au centre de 'arc

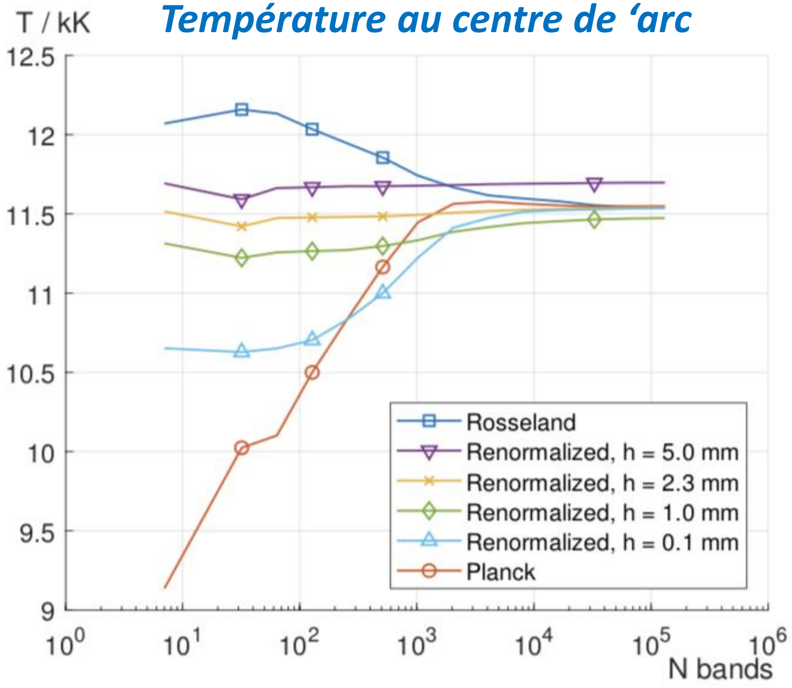

La moyenne de Planck donne le même résultat que Rosseland pour > 10^3 bandes

La fonction renormalisée aboutit à un T(r) acceptable pur H=2.3

SYSTEMATIC INVESTIGATION ON RADIATION MODELING ERRORS OF A WALL-STABILIZED ARC SIMULATIONS

R. FUCHS, H. NORDBORG

Comparaisons effectuées:

Sur le profil de température, température au centre de l'arc en fonction du nombre de bandes, champ E en fonction de nombre de bandes, comparaison NEC et P1 model

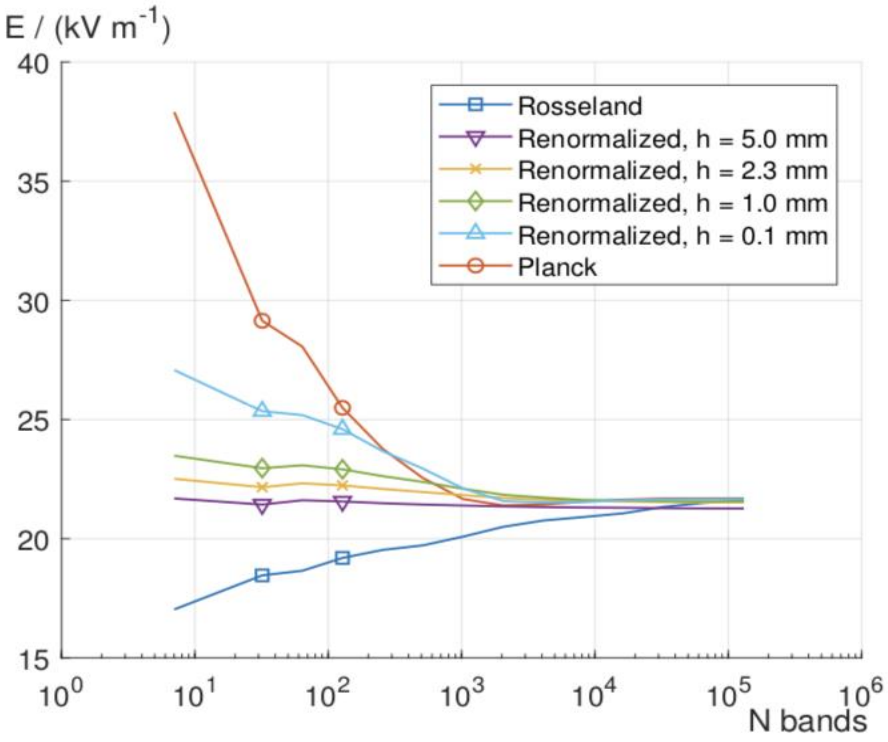

Fig. 3: Arc voltage as spectral domain is refined.

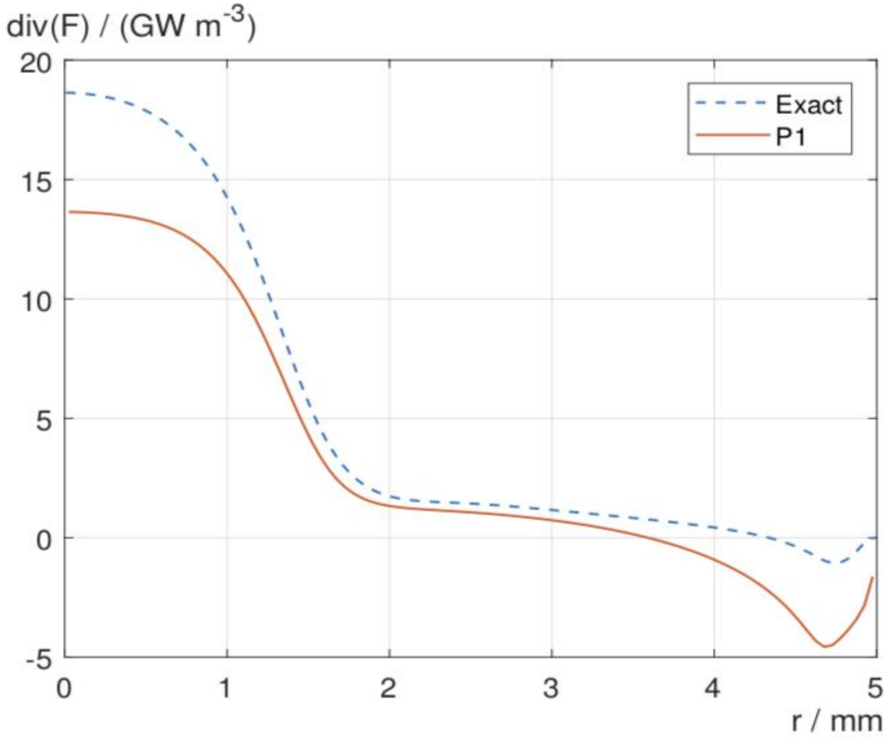

Fig. 4: Net emission computed by exact solution and P1 model.

Conclusion :

7 bandes suffisent pour bien décrire la tension d'arc et le profil T(r) d'un plasma SF_6

COMPARISON OF DIFFERENT MODELS TO CALCULATE THE COMPOSITION AND THERMODYNAMIC PROPERTIES OF A MULTI-TEMPERATURE SF6 PLASMA

X. BAUMANN, P. TEULET, Y. CRESSAULT, G. VANHULLE, F. REICHERT, A. PETCHANKA

Etudes : Comparaison des méthodes de calcul de composition d'un plasma de SF_6 à 2T dans un HVCB
Etude de l'influence sur les propriétés thermodynamiques Cp_e et Cp_g notamment

Théories:

- Plasmas de SF_6, 28 espèces, 109 réactions chimiques

- Définition du paramètre $\theta = T_e/T_g$

- Définition des taux de réactions directs et inverses avec différentes températures →

- Comparaison des méthodes de calcul :
1/minimisation d'une fonction thermodynamique
2/loi d'action de masse (LAM)
3/cinétique chimique, collisionne radiatif couplé aux équations de conservation de la pression

- Système résolu par DVODE library,

- Etude de 2 cas extrêmes : 1/$T_{ex}=T_e$, $T_{vib}=T_e$, $T_{rot}=T_g$ et 2/$T_{ex}=T_g$, $T_{vib}=T_g$, $T_{rot}=T_g$

Table 1. Temperatures T_{tr}, T_{reac} and T_i used in Eq. 2 for different chemical reactions.

Réaction	T_{tr}	T_{reac}	$k_D(T_i)$
$AB + M \rightleftarrows A + B + M$	T_g	T_g	T_g
$A^- + M \rightleftarrows A + e + M$	T_e	T_g	T_g
$A + e + e \rightleftarrows A^- + e$	T_e	T_e	T_e
$A + e \rightleftarrows A^+ + e + e$	T_e	T_e	T_e
$AB + CD \rightleftarrows AC + BD$		T_g	T_g
$A^+ + B \rightleftarrows A + B^+$		T_g	T_g
$AB + e \rightleftarrows A^- + B$		T_g	T_e
$e + A \rightleftarrows B^- + C + D + \cdots$	T_g	T_g	T_g
$e + A \rightleftarrows B + C + D + \cdots + e$	T_g	T_g	T_g
$e + A \rightleftarrows B^+ + C + D + \cdots + e + e$	T_g	T_g	T_g

COMPARISON OF DIFFERENT MODELS TO CALCULATE THE COMPOSITION AND THERMODYNAMIC PROPERTIES OF A MULTI-TEMPERATURE SF6 PLASMA

X. BAUMANN, P. TEULET, Y. CRESSAULT, G. VANHULLE, F. REICHERT, A. PETCHANKA

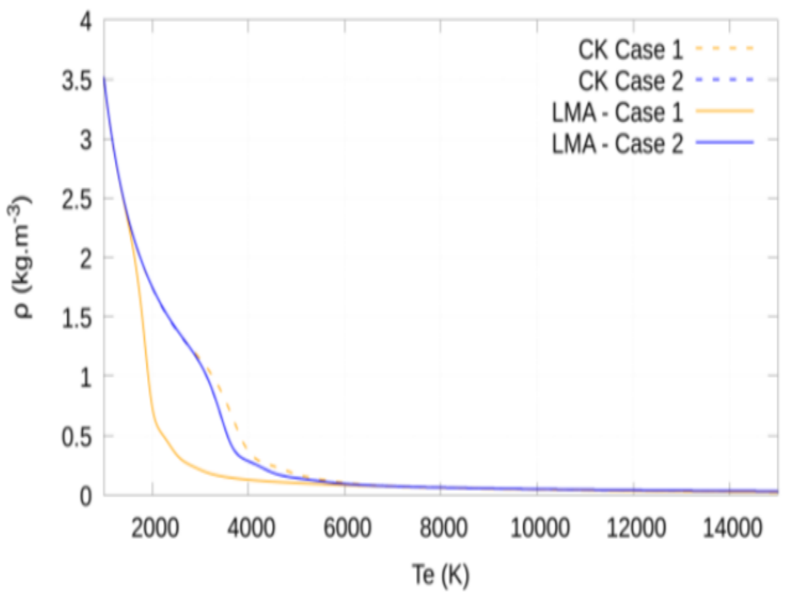

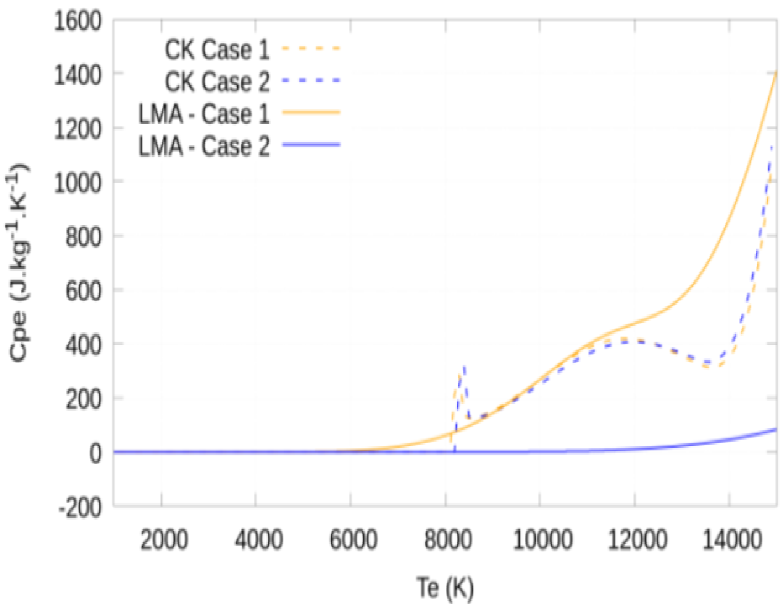

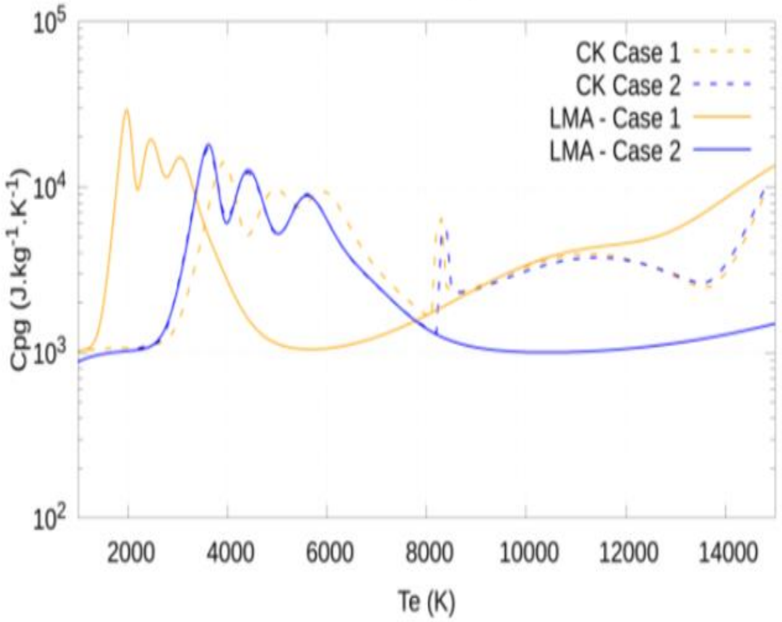

Conclusions

L’étude montre les limites de la LAM pour un milieu non LTE

La LAM est utile pour décrire la composition 2T à hautes températures électroniques T_e, cas 1 (T_e, T_e, T_g)

La LAM est utile pour décrire la composition 2T à basses températures électroniques T_e, cas 2 (T_g, T_g, T_g)

Entre les deux ? La méthode cinétique chimique semble indispensable

Invited lecture

ELECTRIC BREAKDOWN IN HIGH VOLTAGE GAS CIRCUIT BREAKERS

M. SEEGER[1]

[1]ABB Switzerland Ltd, Corporate Research, 5405-Baden Dättwil, Switzerland
*martin.seeger@ch.abb.com

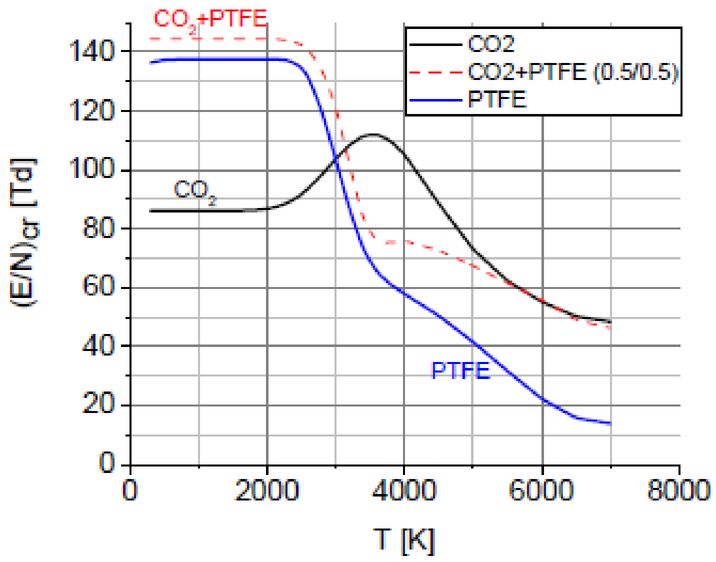

Fig. 3 Particle density reduced critical electric field in CO2 and C_2F_4 (PTFE) mixtures at 1 MPa

RELEVANT PARAMETERS

For gas discharges relevant parameters are the ionisation and electron attachment coefficients.

Invited lecture

BREAKDOWN AT AMBIENT TEMPERATURES

criteria are:
- First electron, i.e. the statistical time lag
- Streamer inception
- Channel heating mechanisms streamer-to-leader transition

the breakdown at rough surfaces can be understood and predicted (ref)

At high pressures, breakdown dominated by dynamic leader propagation effects
(for SF6 - no clear explanations or ref)

Status for CO2 investigation from ABB side: identical to SF6 investigation one

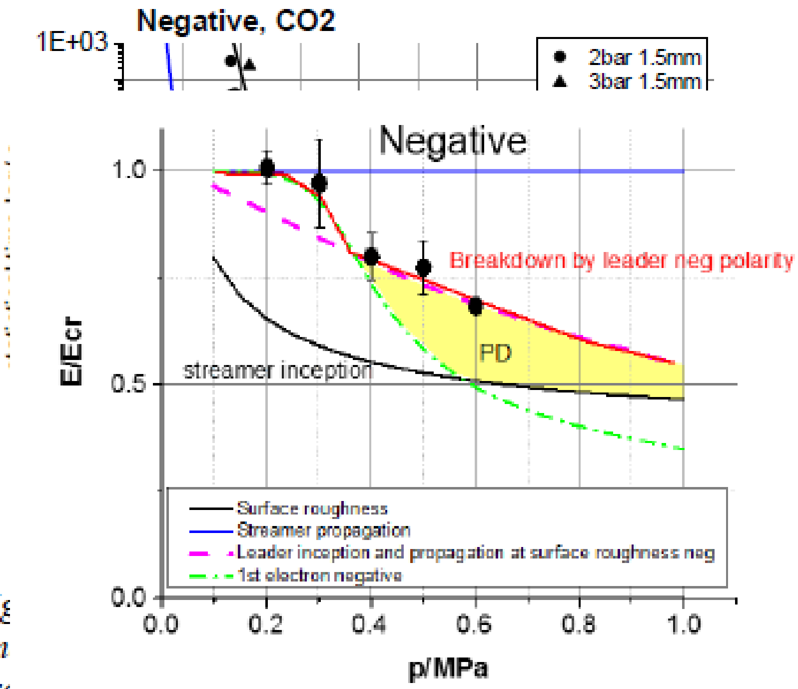

Fig … *at a*
sm … *rious*
pre … *using*
field electron emission [4].

BREAKDOWN AT HIGH TEMPERATURES AFTER CZ

The previously discussed concepts can be applied for the arc interruption at current zero (CZ) or after CZ, during the rise of the transient recovery voltage (TRV).

The breakdown decision times are gas dependent and are in the range of **a few 100 nanoseconds (e.g. SF6) to a few microseconds, (e.g. CO2).**

Several influencing parameters:
the material properties like ρ·cp, the pressure, the turbulent cooling, or also the electron attachment coefficient.

Additionally non-equilibrium effects have to be considered for predictions of the conductance distribution in the arc channel.

[redacted]

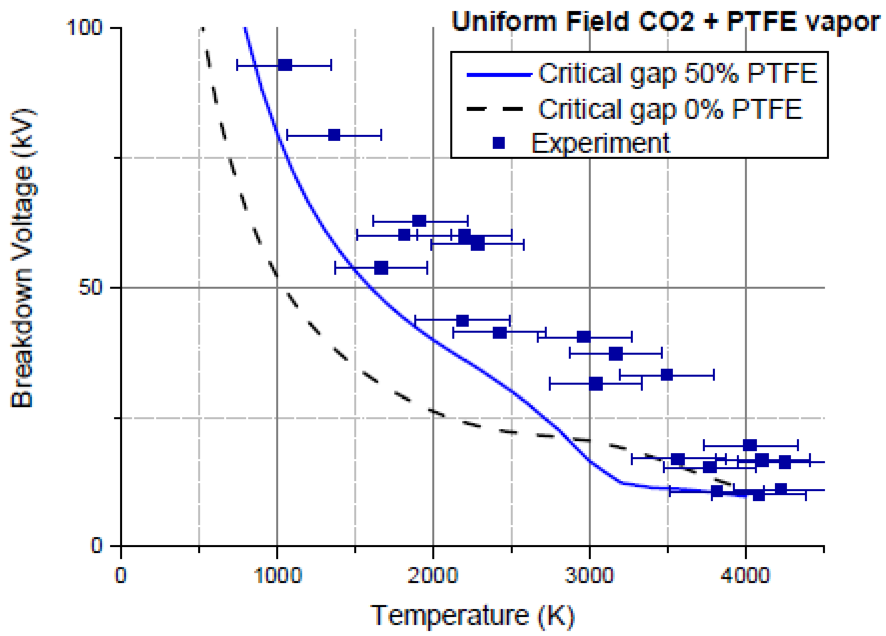

Fig. 9: Breakdown in uniform gap at elevated temperatures in CO_2 at 0.2 MPa with PTFE admixture below 50%. The symbols are the measurements, the curves are predictions based on data from [14].

flow is indicated by the arrows.

Simple contact set up with Teflon gap; no feedback about any experimental erosion measurment

The transition typically happens around 100 µs after CZ

Thermophysical Properties and molecular electrostatic properties of $C_5F_{10}O$ and C_4F_7N

This work was supported by the National Key Basic Research Program of China , National Natural Science Foundation of China and State Key Laboratory of Electrical Insulation and Power Equipment

Yi Wu[1], Chunlin Wang[1], Hao Sun[1*], Zhexin Chen[1]

[1]State Key Laboratory of Electrical Insulation and Power Equipment, *Xi'an Jiaotong University*, China
*sunhao1031@xjtu.edu.cn

"C5F10O and C4F7N which have been shown good insulation, thermal dissipation and switching performances experimentally, have attracted great attention as SF6 alternative gas. "

The plasma composition is calculated based on the local thermodynamic equilibrium using bond energy analysis and theoretically calculated particle partition function and enthalpy of formation, for temperatures ranging **from 300 to 30 000 K at 1 bar**.

Parameters such as the partition function, the enthalpy of formation and the molecular polarizability of the relevant product particles.

Lack of experimental data were calculated using computational chemistry methods.

Gas property studies

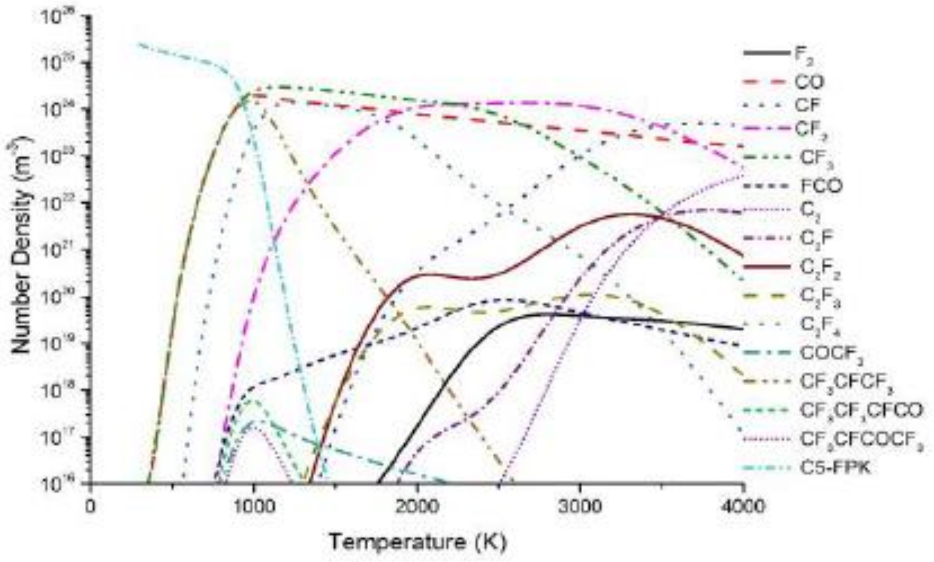

Figure 2. LTE composition of $C_5F_{10}O$ plasma from 300 to 4000 K, only polyatomic species shown.

Thermal conductivity, and product of density and specific heat, C4F7N and C5F10O are closer to SF6 than CO2 and N2.

At near 5000K, **C4F7N and C5F10O have lower electrical conductivity** than SF6.

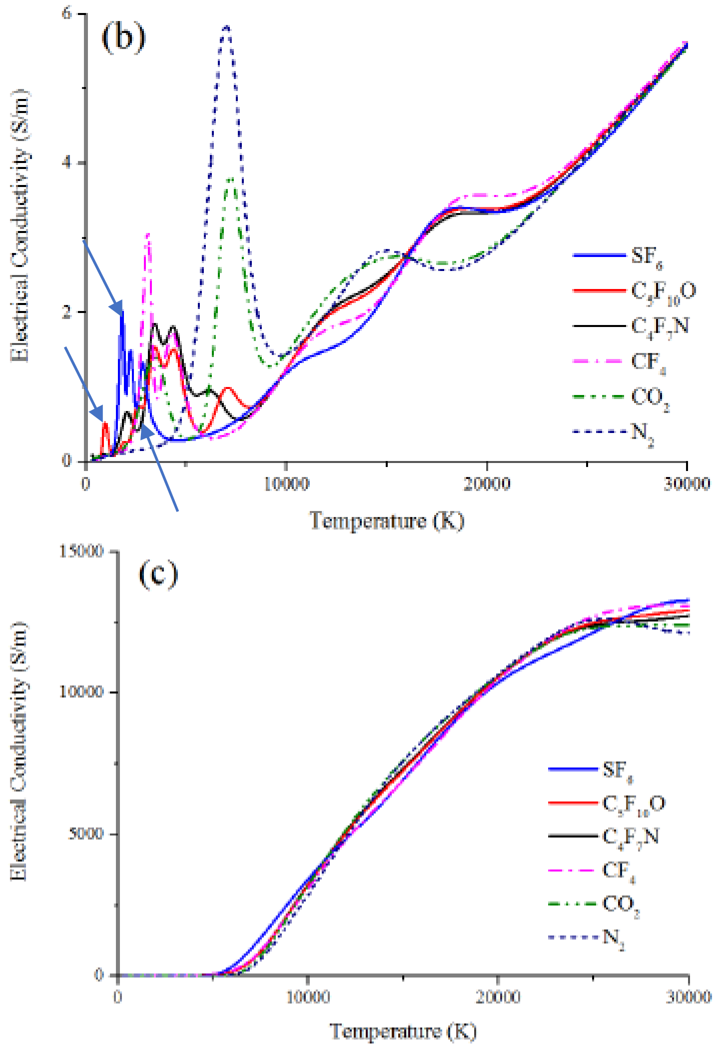

MOLECULAR ELECTROSTATIC POTENTIAL

The molecular electrostatic potential (ESP) V(r) is produced by the atomic nuclei and electrons that constitute the molecule.

Coulomb's law: $$V(r)=\sum_{A}\frac{Z_A}{|R_A-r|}-\int\frac{\rho(r')dr'}{|r'-r|}$$

where ZA is the charge of nucleus A, located at RA, and ρ(r) is the electron density distribution.

Correlation with the dielectric strength of 36 gas molecules which have clear insulation test data:
the larger the positive potential area, the stronger the molecule's ability to attract electrons.

The molecular electrostatic potential has a strict physical definition:
reflects the charge distribution of the molecule itself
good guidance on chemical activity and intermolecular interaction.

Relationship between ESP and molecular insulation properties.

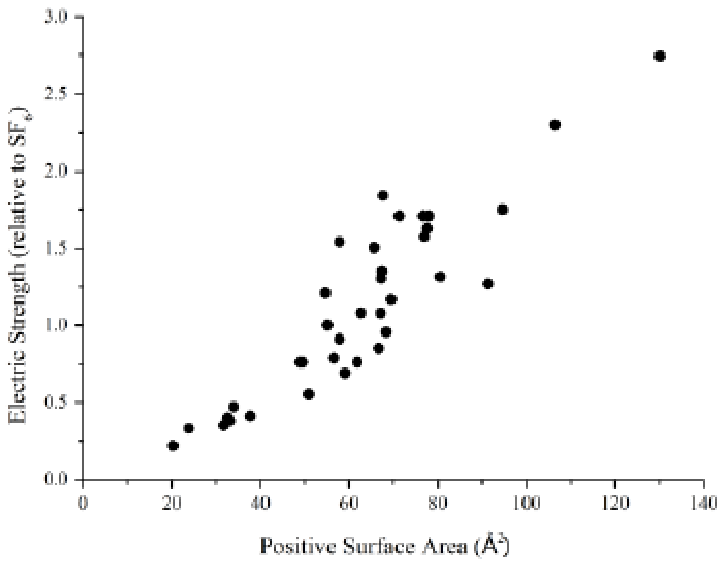

Figure 5. Correlation between electric strength and positive surface area of the 36 particles.

MOLECULAR ELECTROSTATIC POTENTIAL

The molecular electrostatic potential (ESP) V(r) is produced by the atomic nuclei and electrons that constitute the molecule.

Coulomb's law: $$V(r)=\sum_A \frac{Z_A}{|R_A-r|}-\int \frac{\rho(r')dr'}{|r'-r|}$$

where ZA is the charge of nucleus A, located at RA, and ρ(r) is the electron density distribution.

The molecular electrostatic potential has a strict physical definition: reflects the charge distribution of the molecule itself good guidance on chemical activity and intermolecular interaction.

Relationship between ESP and molecular insulation properties.

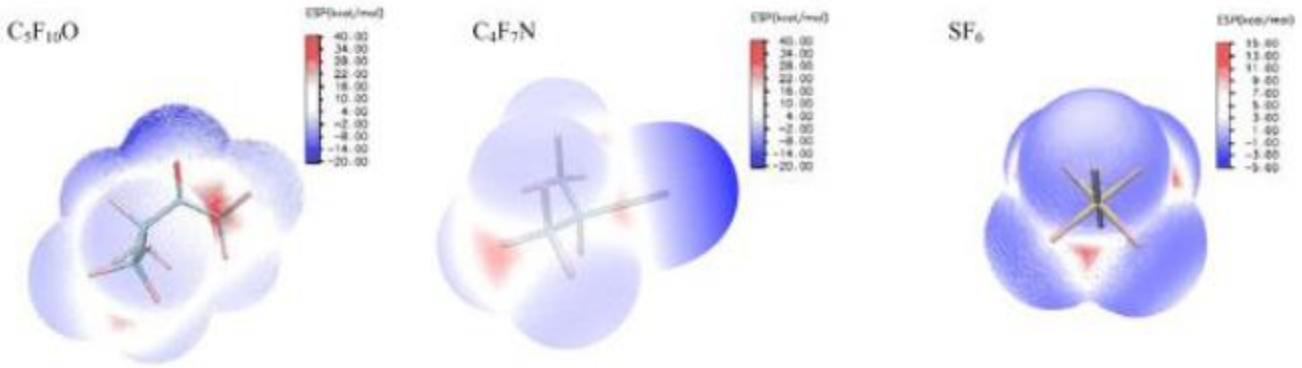

Positive potential is shown in the region near the nucleus, and the negative potential is shown away from the nucleus

Gas property studies L6

Non LTE: cost consuming.

Predicting the dielectric strength by molecular parameters [several ref]:
difficult work because lack of data

Some of the ESP descriptors are strongly correlated, meaning that **there is still much information which was not used.**

Future: to describe qualitatively the interaction between electrons and molecules.

No clear conclusion or the different gases

Gas property studies

Comparison of different models to calculate the composition of a multi-temperatures plasma of SF6
Xavier Baumann, Yann Cressault, Philippe Teulet and Gabriel Vanhulle

1^{st} basic fundamental approach and feasibility

New assumptions to calculate the reaction rates: shows the limits of the law of mass action in ordinary conditions (SF6)

Full detailed analysis of the reaction equations

No direct comparison with current LTE data bases

Effect of optimized / non-optimized Mean Absorption Coefficients on the radiative transfer of Air

N.Kabbaj[1], Y.Cressault[1], P.Teulet[1], F.Reichert[2], A. Petchanka[2]

[1]*Université de Toulouse; UPS, INPT; LAPLACE (Laboratoire Plasma et Conversion d'Energie); 118 route de Narbonne, F-31062, Toulouse Cedex 9, France*

[2] *Siemens AG, E T HP CB PLM R&D B PB, Nonnendammallee 104, 13629 Berlin, Germany*

The calculation and the main results of the radiative properties of Air thermal plasma at *P=1bar*, useful for complete modelling of arc systems. (LTE)

$$\vec{s}\nabla L_\lambda(\vec{r},\vec{s}) = K'(\lambda,T)(B^0{}_\lambda(T) - L_\lambda(T))$$

The selection of the band intervals and the mean function in the calculation of MACs:
critical influence on the accuracy of the radiative flux.

The main objective of this study is to find an **optimal approximate method that allows getting closer to the exact resolution** of the Radiative Transfer Equation (RTE).

Usage of the Modified Planck Mean Function

$$\overline{K}([\lambda_i,\lambda_j],T,R) = \frac{\int_{\lambda_i}^{\lambda_j} K'(\lambda,T)B^0_\lambda(T).exp(-K'(\lambda,T)R)\,d\lambda}{\int_{\lambda_i}^{\lambda_j} B^0_\lambda(T)\,d\lambda}$$

where K' is the monochromatic absorption coefficient **corrected by the stimulated emission** (in m-1), i.e. sum of the monochromatic absorption coefficient of atomic lines, molecular diatomic and polyatomic lines, atomic and molecular continua

R, the characteristic absorption length**, is the optimization parameter**

We conclude that the RTE resolution gives better results. However, this method cannot be used in MHD simulations

Introducing R(t) ?

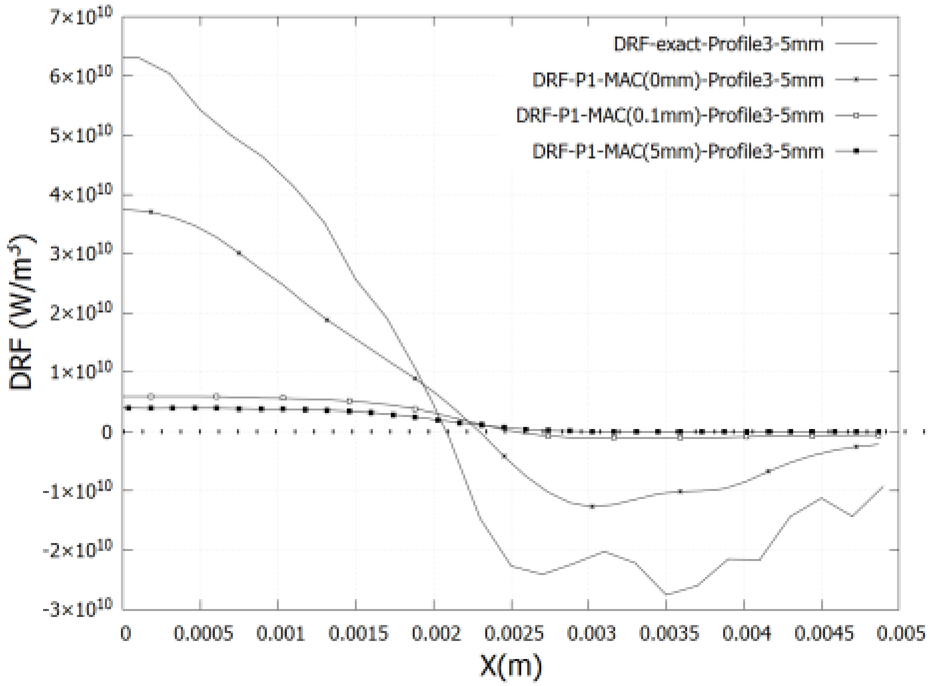

Fig. 5 The exact DRF in comparison with DRF using P1-MAC-(0mm), MAC (0.1mm) and MAC (5mm) for the third temperature profile.

HV/MV/LV CB applications

CFD SIMULATION OF MULTI-COMPONENT REAL-GAS FLOWS IN HIGH VOLTAGE CIRCUIT BREAKER CHAMBERS

SINA ARABI[1*], JEAN-YVES TRÉPANIER[1], RICARDO CAMARERO[1]
PHILIPPE ROBIN-JOUAN[2], PATRICK GUIAVARCH[2] and TIANBO ZHOU[2]

[1]École Polytechnique de Montréal, 2500 chemin de Polytechnique, Montréal, Canada
[2]General Electric, Grid Solutions, 69611 Villeurbanne, France
sina.arabi@polymtl.ca

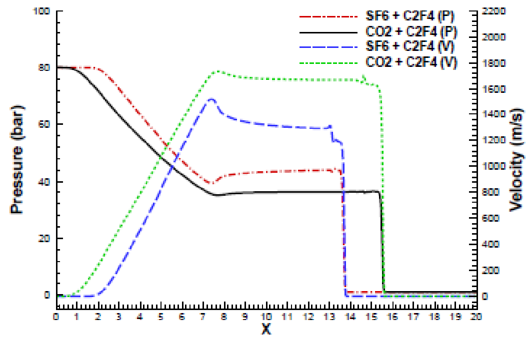

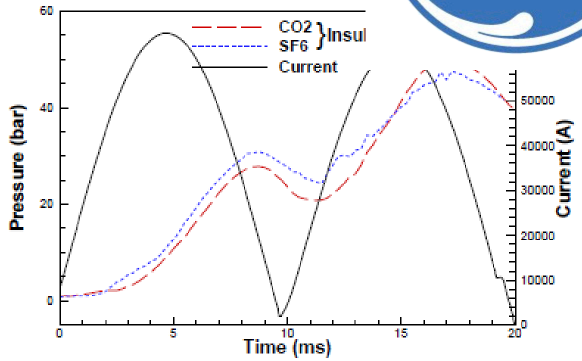

Investigation on the adjunction of O_2 in g^3 and its impact on dielectric and breaking in high voltage circuit breaker

K. Bousoltane[1], Y. Kieffel[1], T. Berteloot[1] , Ph Robin-Jouan[1], D. Vigouroux[1] , Ph. Teulet[2]

[1] *GE, Villeurbanne, 69100, France*
[2] *Laplace, Toulouse, France*

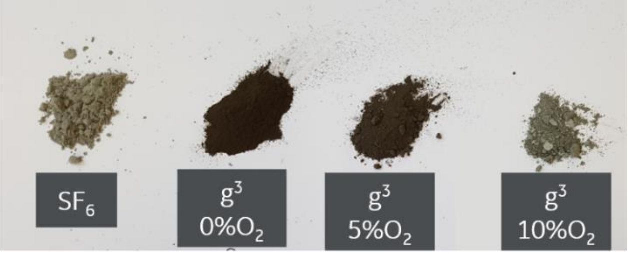

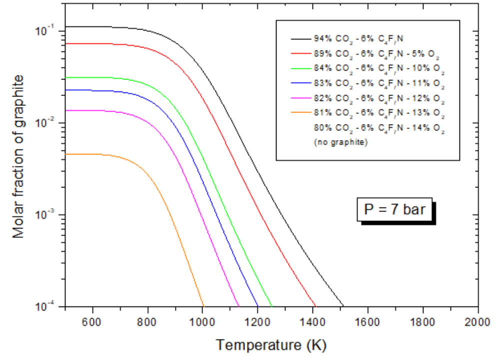

LAST DEVELOPMENT RESULTS FOR 170kV CIRCUIT-BREAKER PROJECT USING g^3 GAS

H.E. JUNG[1], K.K. OH[1], Y.G. KIM[1], K. BOUSOLTANE[2],
M. PERRET[2], P. ROBIN-JOUAN[2*], J-Y. TREPANIER[3], S. ARABI[3]

[1] LSIS, CheongJu, Korea
[2] GE Grid Solutions, Villeurbanne, France
[3]Ecole Polytechnique de Montréal, Québec, Canada

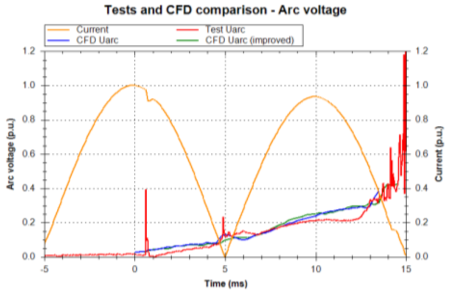

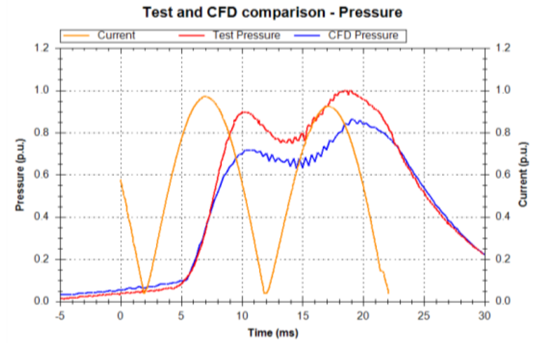

CFD SIMULATION OF A 3D FEATURED ELECTRICAL ARC CONFIGURATION IN A 2D AXISYMMETRICAL SIMULATION DOMAIN

A. PETCHANKA[1]*, F. REICHERT[1]

[1] Siemens AG, Nonnendammallee 104, Berlin, 13629, Germany
arkadz.petchanka@siemens.com

Alternative 2D axisymmetrical simulation approach on the example of an electrical disconnector

From large distances from the axial symmetry: completely changes for the arc attachment
The arc voltage is affected by such transformation.

~~Assumption of the **arc current** conservation~~

Assumption of the conservation of the **arc attachment size**

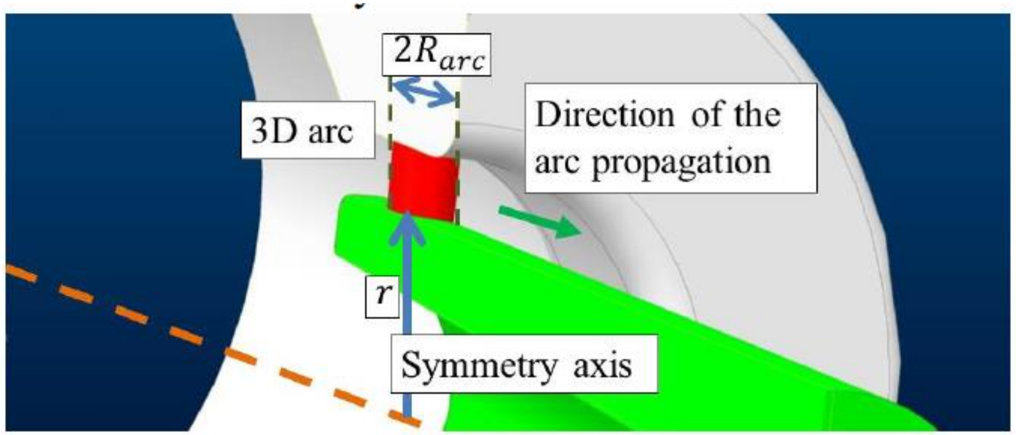

Fig. 1: *3D arc configuration*

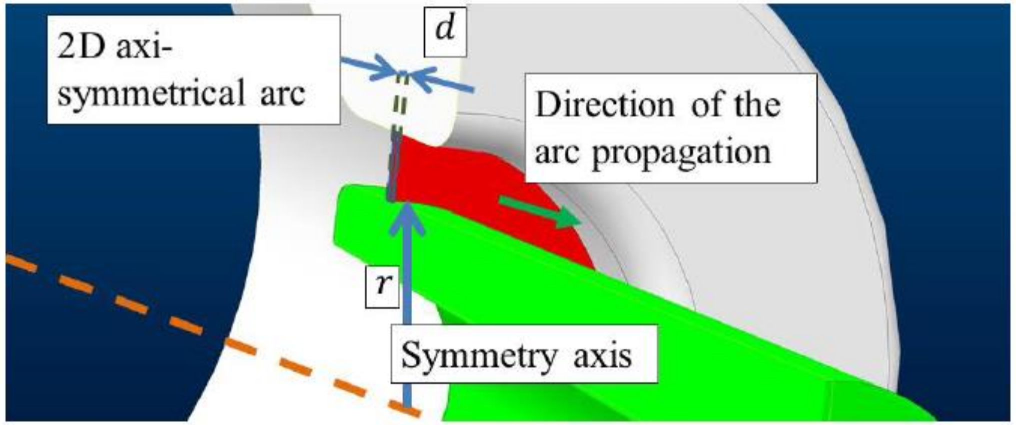

HV/MV/LV CB applications A13

$$I_{2D} = kI,$$

$$j_{2D} = j_{3D} = j, d = 2R_{arc}.$$

$$\frac{kI}{4\pi r R_{arc}} = \frac{I}{\pi R_{arc}^2} \Longrightarrow k = \frac{4r}{R_{arc}}.$$

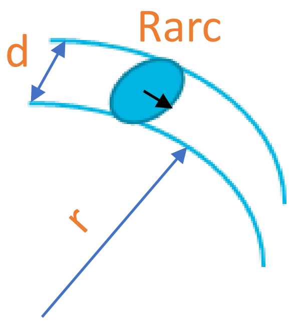

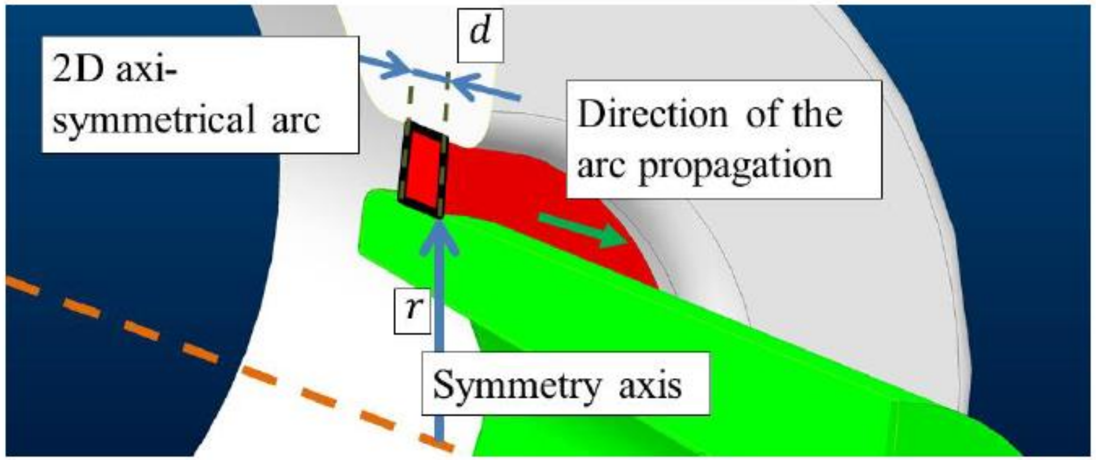

The calculation of the scaling factor **k requires the knowledge of the arc attachment radius Rarc**.
Evaluated in advance by means of the following numerical experiment

ANSYS calculations (Navier-Stokes, MHD, DOM modelling)

The numerical evaluation of Rarc has yielded in nearly the constant **Rarc 0:4mm** during the main part of the duration of the interruption current

k = 190: the arc current in 2D axisymmetrical geometry must be 190 time higher in order to obtain the same arc width

2D equivalent sections

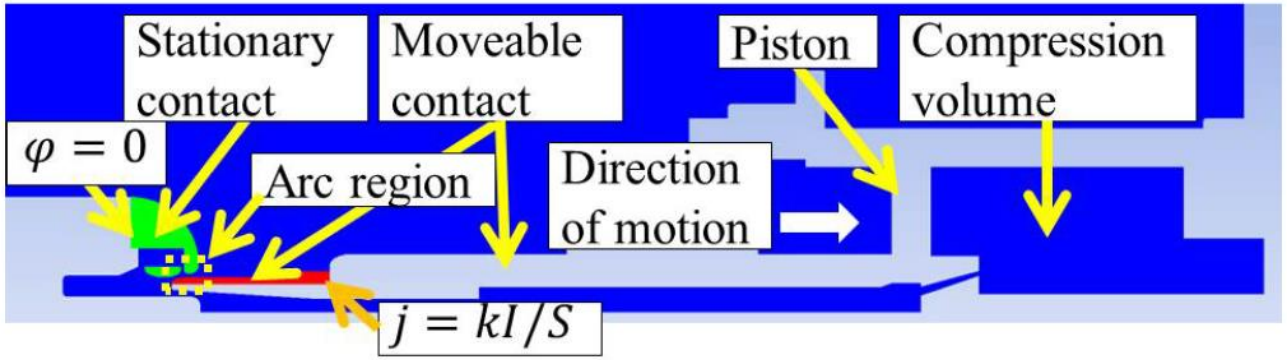

Simulation domain of the disconnector

In order to not overestimate the Lorentz forces caused by the native interruption current, **the magnetic field induced by the scaled current kI has been divided by the scaling factor k**.

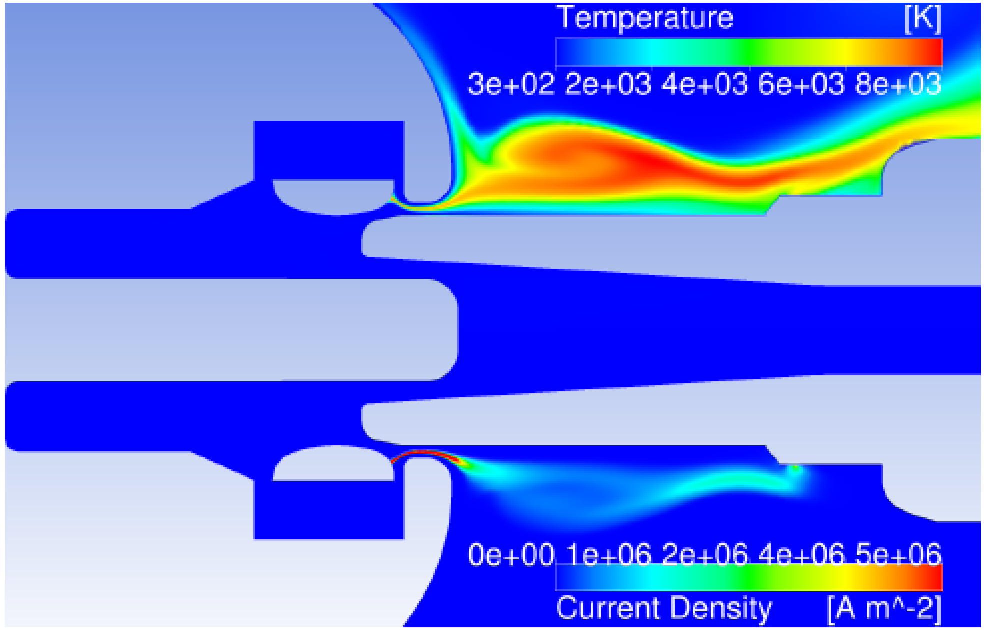

Fig. 9: *Temperature and current density distribution at* $t = 7.7ms$ *after the contact separation*

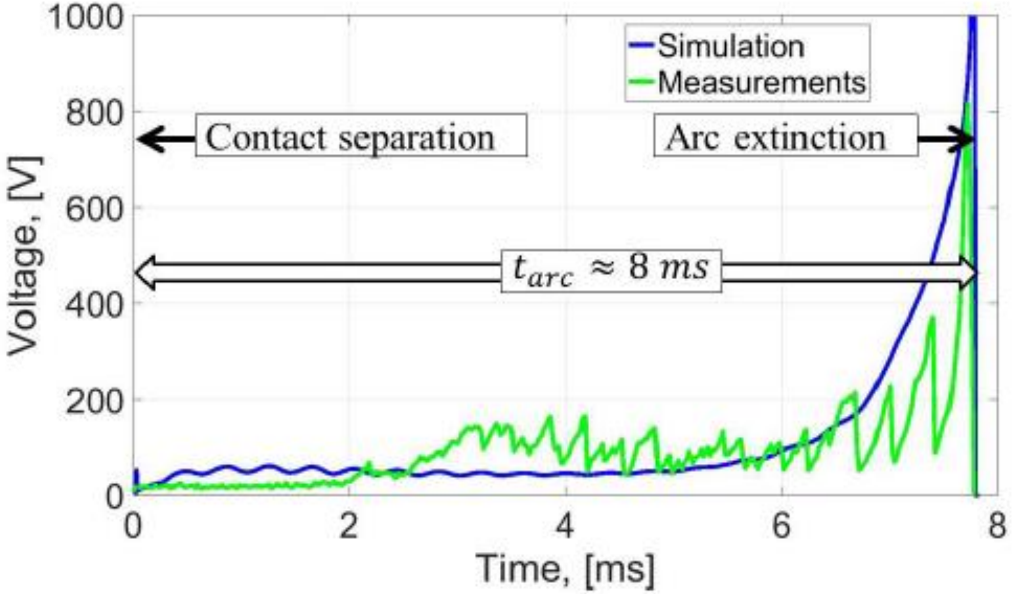

No gas flow comparisons between the 2 approaches
No overpressure comparisons: been assumed they are similar
Full 3D is required for more accuracy.

Approach to be discussed
Concept or fictitious electrode more appropriate (for axial situation)

COMPARISON OF THE ARC CHARACTERSITICS AND ARC QUENCHING CAPABILITIES BETWEEN CO_2 AND SF_6 IN HIGH-VOLTAGE GAS CIRCUIT BREAKERS

Z. GUO[1], X.W. LI[1]*, L. CHEN[1], J.Y. XIONG[1], S.L. JIA[1]

[1]State Key Laboratory of Electrical Insulation and Power Equipment,
Xi'an Jiaotong University, 710049, Xi'an, China
*xwli@mail.xjtu.edu.cn

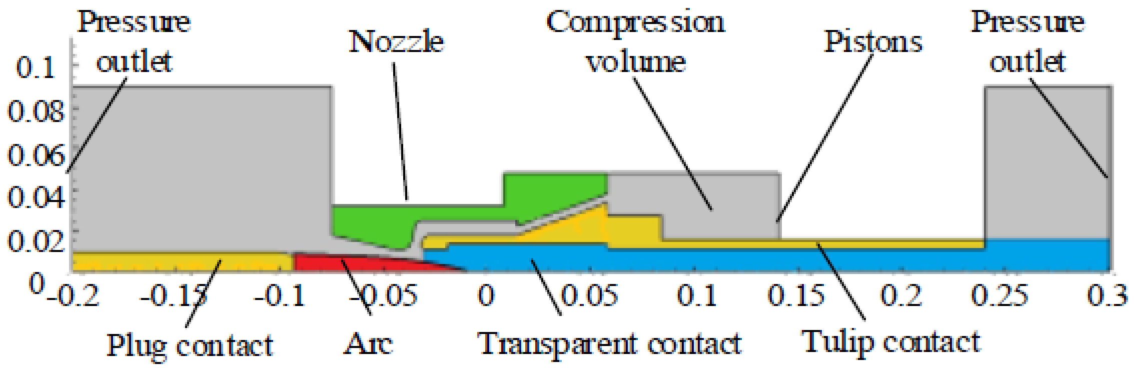

(MHD) arc model (+ NEC) for a puffer type 126 kV high-voltage circuit breaker
Different arc quenching mediums of CO2 and SF6 at 0.6 MPa.

The thermodynamic and transport properties of CO2 are taken from the study of Tanaka

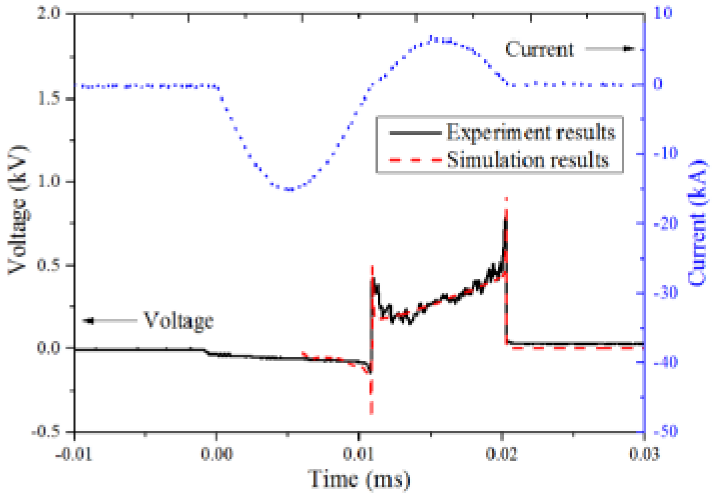

(a) CO_2

The results
increases w

The simula ... ance
for the CC ... filling
pressure is

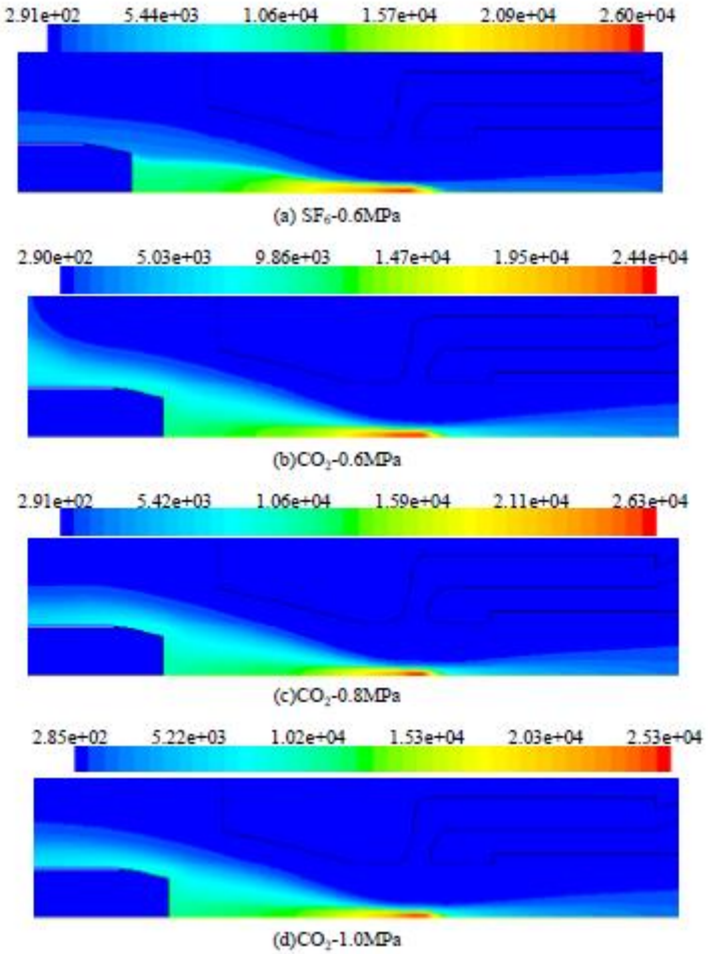

Fig.4 The temperature distributions in the arc area at 0.5ms before the current-zero with different mediums and different filling pressures.

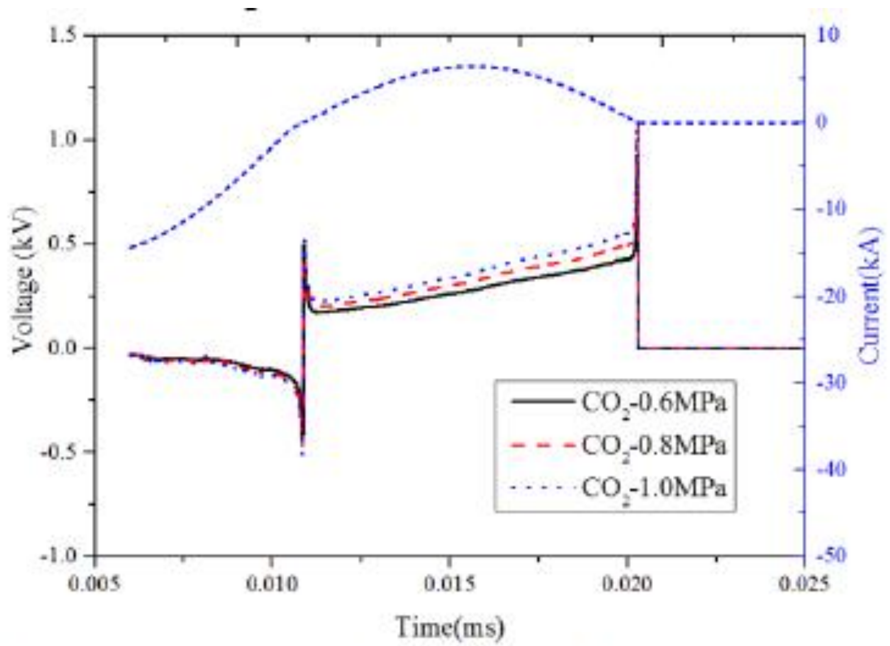

Fig.3 Simulated arc voltage for the CO_2 interruption process with different filling pressures

HV/MV/LV CB applications A23

CO2: **the temperature at the arc core becomes lower when the filling pressure is higher.**

The arc radius, defined as the position of the 4000K isotherm decreases with the increase of the filling pressure.

The temperature at the arc core of the SF_6 arc is higher than that of the CO_2 arc

The arc radius of the SF_6 is smaller, which is caused by the different ρC_p of SF_6 and CO_2 (which is smaller)

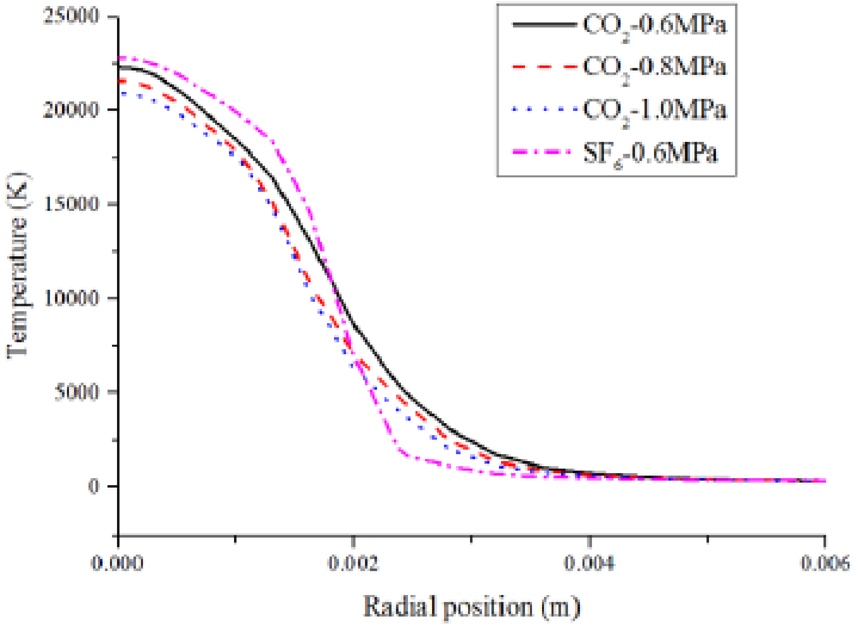

Fig.5 The temperature distribution along the radial direction at the nozzle throat and at 0.5ms before the current-zero with different mediums and different filling pressures.

$$\frac{1}{g}\frac{dg}{dt}=\frac{1}{\theta}\left(\frac{u\cdot i}{Q}-1\right)$$

$$\theta=\frac{g_1 i_2^{\,2}-g_2 i_1^{\,2}}{i_1^{\,2}\frac{dg_2}{dt}-i_2^{\,2}\frac{dg_1}{dt}}$$

$$Q=\frac{i_2^{\,2}\frac{dg_1}{dt}-i_1^{\,2}\frac{dg_2}{dt}}{g_2\frac{dg_1}{dt}-g_1\frac{dg_2}{dt}}$$

assuming that the time constant θ and the cooling power Q keep constant within a simulation time step.

θ and Q at a specific time can be obtained by using two adjacent time steps

The interruption capability increases with the increase of the filling pressure.

With the increase of the filling pressure, the θ decreases and the Q increases

However, the interruption performance of CO_2 at 1.0MPa is still lower than that of SF_6 at 0.6MPa.

The interruption capabilities for CO_2 at 0.6 MPa, 0.8 MPa and 1.0 MPa are about 47%, 76% and 95% of SF_6 at 0.6 MPa

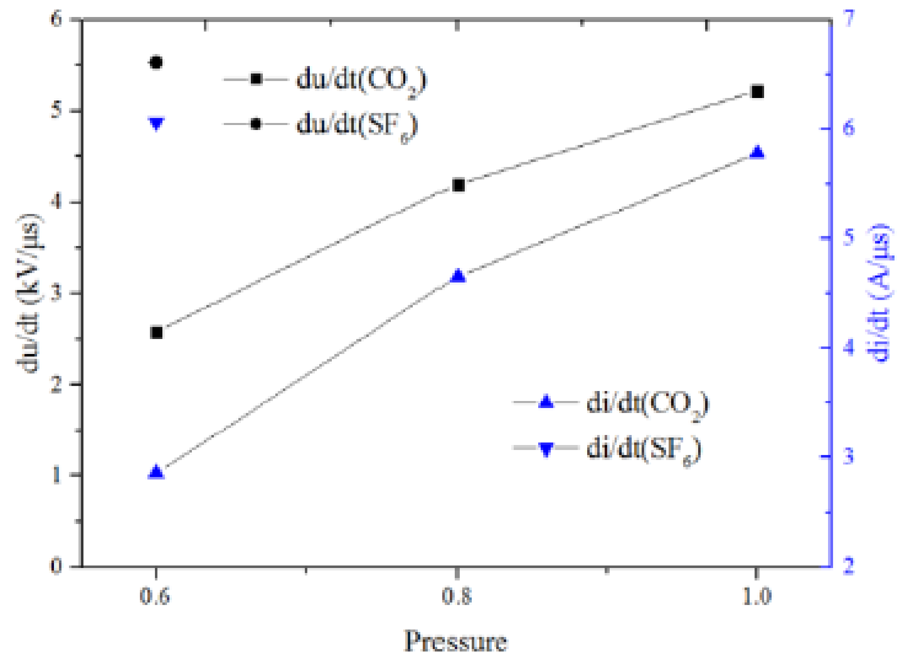

Fig.8 The critical du/dt and di/dt for different mediums and different filling pressures.

PROPERTIES OF CO_2/O_2 GAS MIXTURE AS AN ALTERNATIVE MEDIUM FOR GAS CIRCUIT BREAKERS

A. MAJIMA[1*], T. UCHII[1], T. YASUOKA[1] T. INOUE[2] AND D. SCHIFFBAUER[3]

[1] Toshiba Corporation, Kawasaki 210-0862, Japan
[2] Toshiba Energy Systems & Solutions Corporation, Kawasaki 210-0862, Japan
[3] Toshiba International Corporation, Houston TX 77041, USA
*amane.majima@toshiba.co.jp

Description of the key properties of the CO2/O2 gas mixture as one possible candidate of natural alternative gases to SF6.

From a purely thermodynamic perspective, **higher operating pressures of CO2/O2 may be achieved** while maintaining saturation temperatures even at -50 deg.C

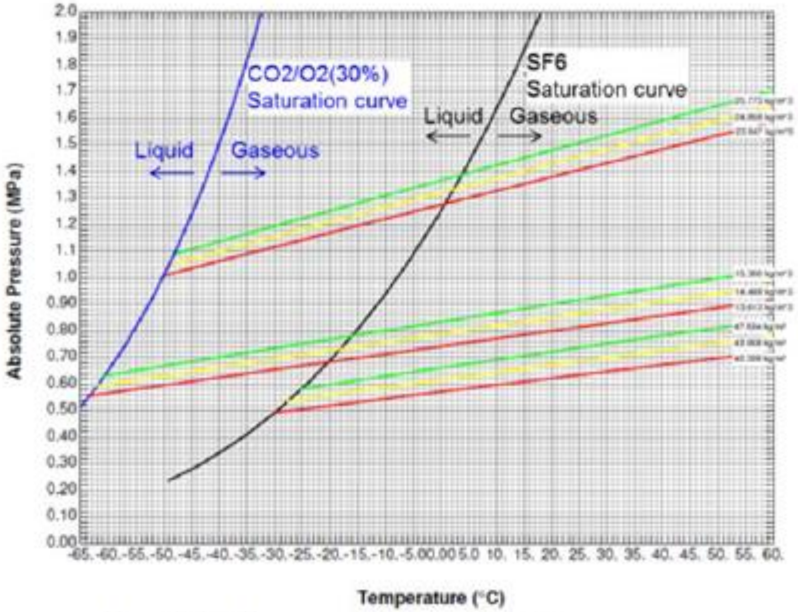

Fig. 1 T-P diagram of SF_6 and CO_2/O_2 mixture.

Theoretical withstand

*E*cr of CO2/O2 mixture was obtained by zero dimensional electron analysis

Addition of O2 to CO2 (base gas) is beneficial for electrical insulation

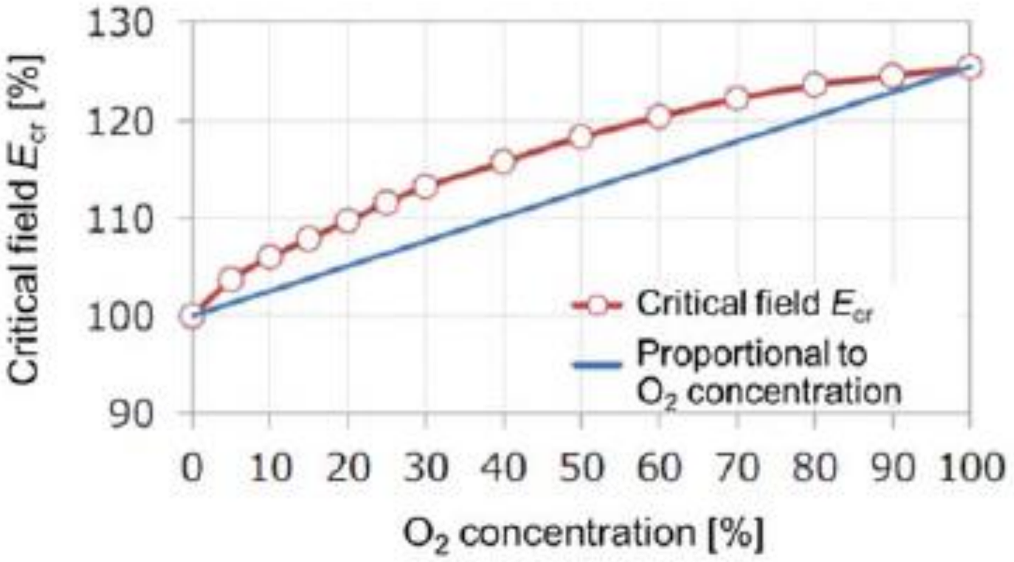

Fig. 2 Theoretical critical electrical field of CO_2/O_2 mixture.

HV/MV/LV CB applications D6

Interruption performance:
more O2 concentration can give so much better thermal interruption performance

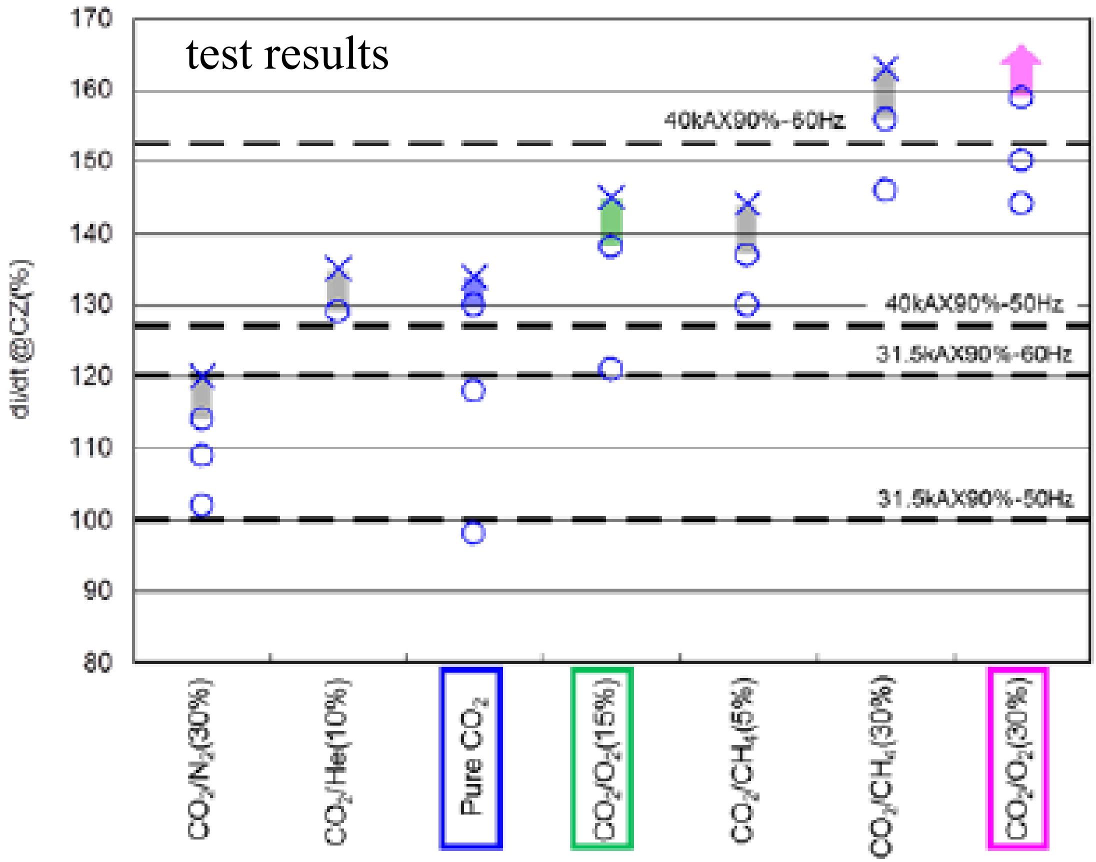

Fig. 3 Comparison of thermal interruption performances among several CO_2-based natural gas mixtures. (0.8 MPa-abs, 90% short line fault)

HV/MV/LV CB applications D6

Dielectric performance
addition of O2, as well as elevated pressure, could potentially enhance dielectric interruption performance (+30% between 0% and 30%)
(no ref)

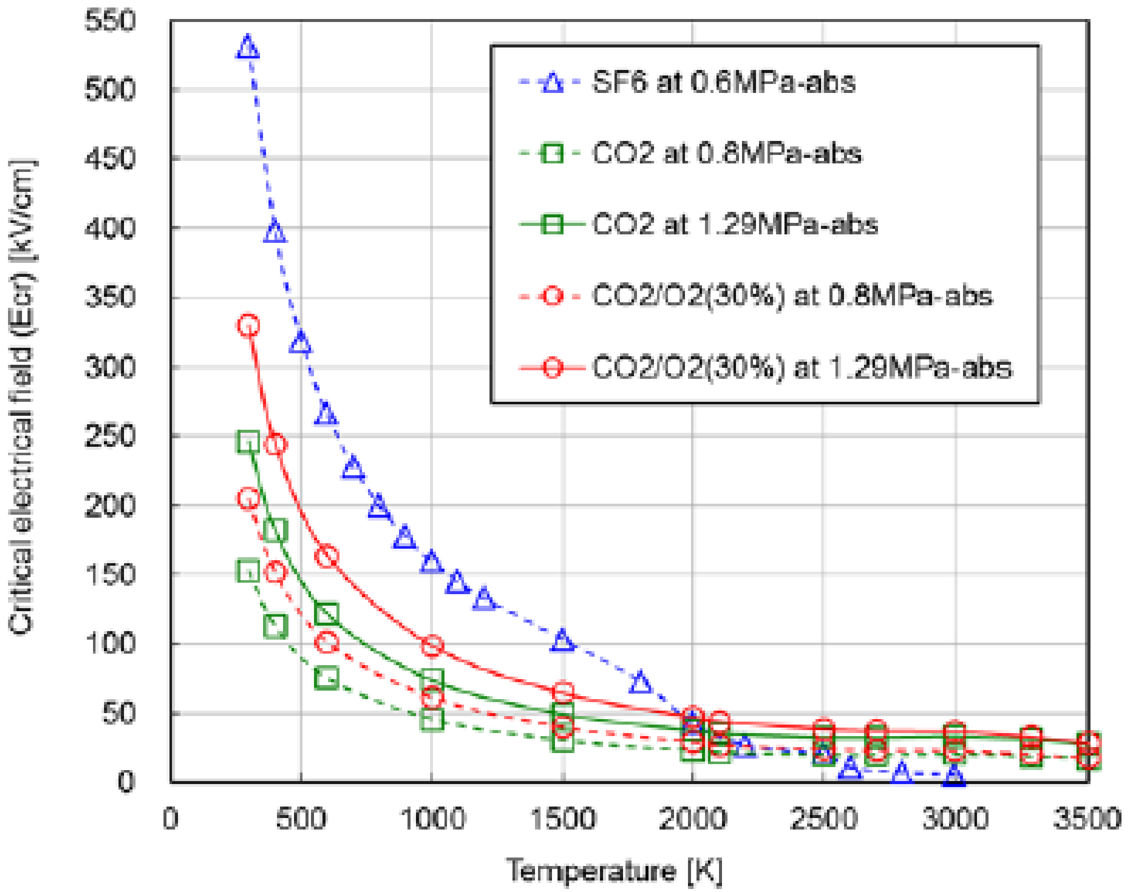

Fig. 4 Theoretical hot gas dielectrics for various gases and pressures. [4]

COOLING PERFORMANCE

additional +20% O2 concentration brings about -11% to -8% reduction of temperature rise
(no ref about measurement conditions)

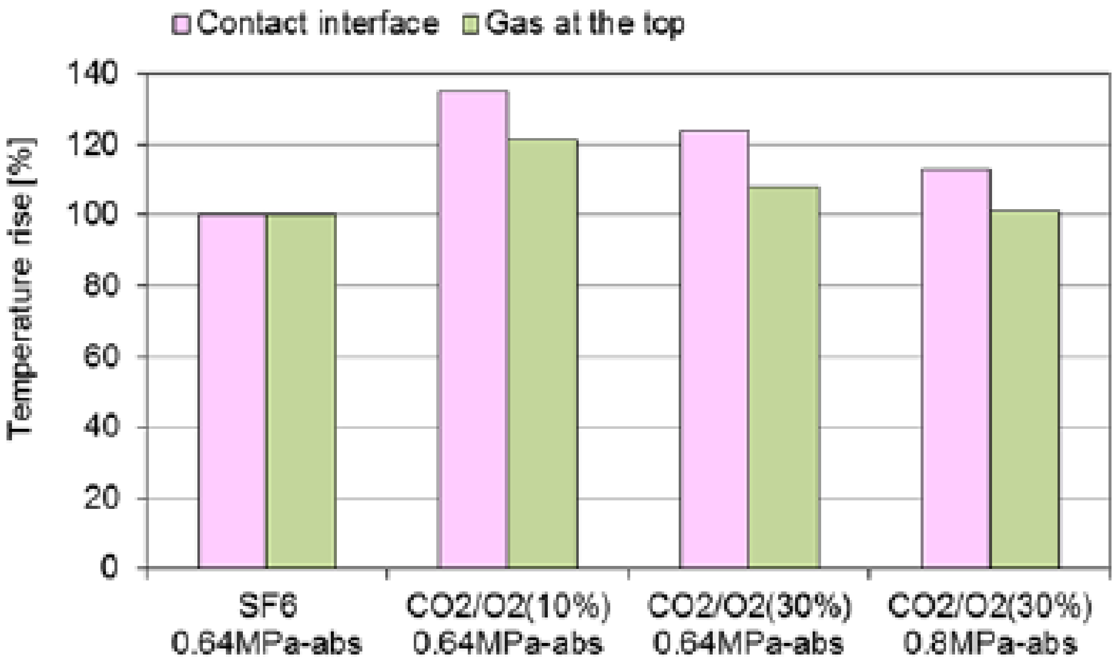

Fig. 5 Temperature rise test results for several gases and pressures. (horizontal co-axial bus bar model, 2,000 A)

HV/MV/LV CB applications D6

DECOMPOSED GASES AND SOLID BY-PRODUCTS AFTER ARCING

30% O2 drastically reduces CO generation

HF is also a concern but may be managed with suitable absorbent as has been well proven with traditional SF6 switchgear.

Table 2 Decomposed gases after arcing in pure CO_2 and CO_2/O_2 mixture. (31.5 kA x 8 shots, 0.8 MPa-abs)

(Unit: ppmV)

	Toxicity LC50	Pure CO_2	CO_2/O_2(30%)
CO_2	470,000/0.5h	(Balance)	(Balance)
O_2	-	196	(Balance)
CO	1,659-1,805/4h	5,909	110
HF	650/4h	~100	~100
H_2	> 15,000/1h	15	4
CH_4	> 500,000/2h	2	2

Pure CO_2 (Dark-brownish) | CO_2/O_2(30%) (Whitish)

Fig. 6 Solid by-products after arcing in pure CO_2 and CO_2/O_2 mixture. (31.5 kA x 8 shots, 0.8 MPa-abs)

MATERIAL COMPATIBILITY

A negative aspect of the CO2/O2 mixture application may be acceleration of material aging due to radical nature of O2

Erosion rate of the plug contact:
almost equivalent and those of the nozzle and the tulip contact for both lower with higher O2 concentration.

Physical interpretations:
require very complicated analysis due to the dynamic and transient nature of the phenomena

Conclusion:
additional O2 up to at least 30% did not cause any significant negative effect on erosion of PTFE nozzle and W/Cu arcing contact materials.

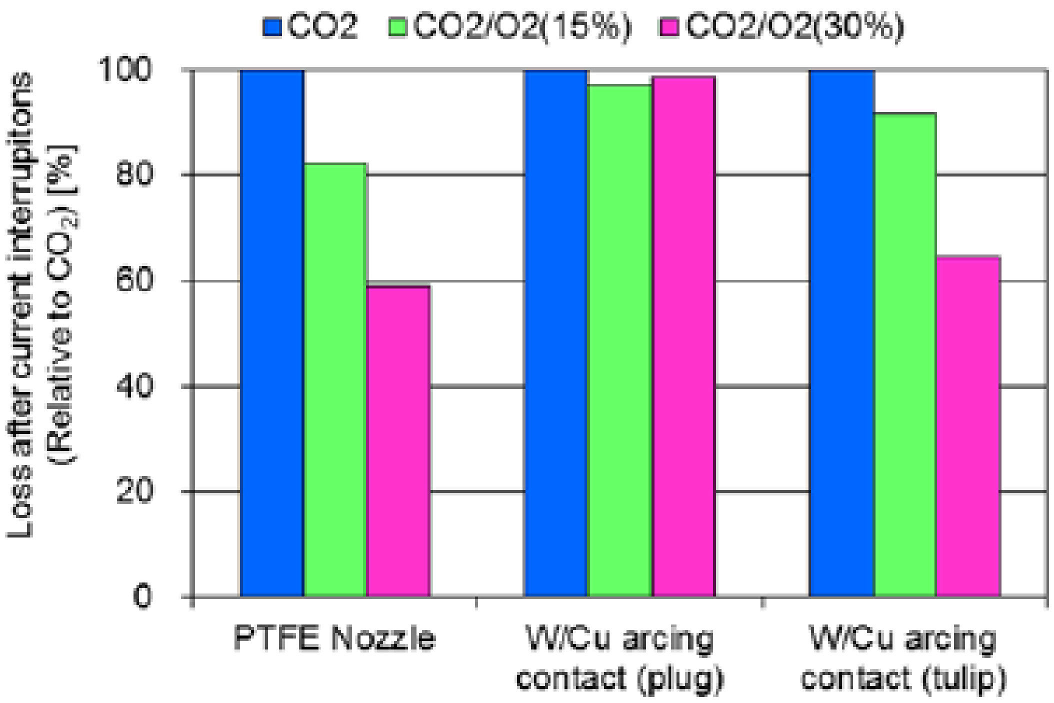

Fig. 7 Comparison of erosion rates of PTFE nozzle and W/Cu arcing contact materials among different O_2 concentrations. (23-29 kA x 12 shots, 0.8 MPa-abs)

Conclusions

High quality for papers
Strong young presence (Asia)

High focus on SF6 replacement topics
Many CO2 papers

Few about HVDC

Workshops: to be revised in terms of organization (no real discussions)

Next GD 2020 in Greifswald (Germany)

Proceedings available by Ph RJ


bambi
plazma®
PLAZMA®

plazma plus
CAPPUCCINO
plazma plus
ČOKOLADA
plazma plus
LEŠNIK